Geoscience Frontiers 11 (2020) 303–324

HOSTED BY

Contents lists available at ScienceDirect

China University of Geosciences (Beijing)

Geoscience Frontiers

journal homepage: www.elsevier.com/locate/gsf

Research Paper

New insights from low-temperature thermochronology into the tectonic and geomorphologic evolution of the south-eastern Brazilian highlands and passive margin

Gerben Van Ranst [a,*], Antônio Carlos Pedrosa-Soares [b], Tiago Novo [b], Pieter Vermeesch [c], Johan De Grave [a]

[a] Laboratory for Mineralogy and Petrology, Department of Geology, Ghent University, Krijgslaan 281 S8, 9000, Ghent, Belgium
[b] CPMTC, Institute for Geosciences, Federal University of Minas Gerais, Avenida Antônio Carlos 6627, CEP 31270-901, Belo Horizonte, Brazil
[c] Department of Earth Sciences, University College London, 5 Gower Place, WC1E 6BS, London, United Kingdom

ARTICLE INFO

Article history:
Received 15 December 2018
Received in revised form
10 May 2019
Accepted 23 May 2019
Available online 13 June 2019
Handling Editor: M. Santosh

Keywords:
Tectonic reactivation
Differential denudation
Passive margin
South-eastern Brazil
Apatite fission tracks
Apatite (U–Th)/He

ABSTRACT

The South Atlantic passive margin along the south-eastern Brazilian highlands exhibits a complex landscape, including a northern inselberg area and a southern elevated plateau, separated by the Doce River valley. This landscape is set on the Proterozoic to early Paleozoic rocks of the region that once was the hot core of the Araçuaí orogen, in Ediacaran to Ordovician times. Due to the break-up of Gondwana and consequently the opening of the South Atlantic during the Early Cretaceous, those rocks of the Araçuaí orogen became the basement of a portion of the South Atlantic passive margin and related south-eastern Brazilian highlands. Our goal is to provide a new set of constraints on the thermo-tectonic history of this portion of the south-eastern Brazilian margin and related surface processes, and to provide a hypothesis on the geodynamic context since break-up. To this end, we combine the apatite fission track (AFT) and apatite (U–Th)/He (AHe) methods as input for inverse thermal history modelling. All our AFT and AHe central ages are Late Cretaceous to early Paleogene. The AFT ages vary between 62 Ma and 90 Ma, with mean track lengths between 12.2 μm and 13.6 μm. AHe ages are found to be equivalent to AFT ages within uncertainty, albeit with the former exhibiting a lesser degree of confidence. We relate this Late Cretaceous–Paleocene basement cooling to uplift with accelerated denudation at this time. Spatial variation of the denudation time can be linked to differential reactivation of the Precambrian structural network and differential erosion due to a complex interplay with the drainage system. We argue that posterior large-scale sedimentation in the offshore basins may be a result of flexural isostasy combined with an expansion of the drainage network. We put forward the combined compression of the Mid-Atlantic ridge and the Peruvian phase of the Andean orogeny, potentially augmented through the thermal weakening of the lower crust by the Trindade thermal anomaly, as a probable cause for the uplift.

1. Introduction

Passive margins represent the transition of continental lithosphere to oceanic lithosphere within the same plate. This is expressed through a major transition in, amongst others, density, rheology and crustal (elastic) thickness. The evolution of a passive margin is inherently linked to the geological record of the neighbouring sedimentary basins. This setting makes passive margins predisposed to be influenced by processes both from the oceanic and continental domains, which are then registered in its landscape and in the stratigraphy of the adjacent basins. A feature that is often observed at passive margins around the world is the presence of a high elevation (1–2 km), low-relief plateau, characterised by an escarpment towards the coastal plain and/or with steeply incised valleys (Japsen et al., 2012b; Green et al., 2018). Passive margins however vary strongly in morphology, from exhibiting this low-

* Corresponding author.
E-mail addresses: gerben.vanranst@ugent.be (G. Van Ranst), pedrosasoares@gmail.com (A.C. Pedrosa-Soares), tiagoanovo@gmail.com (T. Novo), p.vermeesch@ucl.ac.uk (P. Vermeesch), johan.degrave@ugent.be (J. De Grave).
Peer-review under responsibility of China University of Geosciences (Beijing).

https://doi.org/10.1016/j.gsf.2019.05.011

relief plateau with strongly expressed escarpment either close or further (>100 km) away from the coast, to lower plateaus with higher relief or even total absence of an escarpment altogether.

With the introduction of isostatic models (e.g. McKenzie, 1978), it was recognised that passive margins and their basins are strongly coupled in terms of flexural isostasy (Gilchrist and Summerfield, 1990; Rouby et al., 2013). In this view, the elevated plateaus observed at many passive margins across the globe are believed to be an enduring remnant of break-up (e.g. Weissel and Karner, 1989; Gilchrist and Summerfield, 1990; Kooi and Beaumont, 1994; Brown et al., 2002). Other studies on passive margins throughout the last 20 years however illustrated a totally different idea on passive margins, revealing tectonic activity (long) after break-up (e.g. Cobbold et al., 2001; Raab et al., 2002; Fetter, 2009; Cogné et al., 2012; Japsen et al., 2012a,b). Moreover, the elevated platforms at passive margins were found to have a young origin and clearly arose after break-up (Turner et al., 2008; Japsen et al., 2012a,b). However, whether the high elevation features and escarpments are perennial since or before rifting, or rather the product of younger tectonics, remains a source of debate (Braun, 2018).

While nowadays it is clear that the term 'passive margin' is a poorly chosen one, backed by a multitude of observations that evidence post-break-up tectonic activity at these margins, there is still no consensus on the geodynamic context that produces this intraplate tectonic activity (Green et al., 2018). At the source of this debate lies the complex thermal history of a passive margin, including diverse thermal processes and interactions taking place since break-up initiated, combined with multiple phases of uplift and subsidence. The geomorphology that forms as an outcome is further controlled by the intricate interplay between lithology, regional structures and erosive processes.

Information about the geological history of passive margin is often retrieved by thermochronology (e.g. Gallagher et al., 1994; Gallagher and Brown, 1997; Brown et al., 2002; Cogné et al., 2011, 2012; Green et al., 2013; Japsen et al., 2016; Wildman et al., 2016) or structural and landscape modelling (e.g. Leroy et al., 2008; Sacek et al., 2012; Braun et al., 2013; Rouby et al., 2013; Braun, 2018), often combined with information from offshore basin stratigraphy, geomorphology and/or geophysical well data. Different local or plate-wide forces are indicated to explain post break-up tectonic activity, including continental and ocean ridge stresses, mantle plumes, dynamic topography and climate control. Green et al. (2018) argue for one universal process lying at the base of the tectonic reactivation and recently proposed seven points to elucidate the geodynamic evolution of passive margins. A review on numerical modelling approaches to explain escarpment evolution at passive margins was also recently published by Braun (2018).

A large portion of the south-eastern Brazilian highlands (~15°S and 21°S) and the continental passive margin facing the South Atlantic Ocean is floored by the rocks of the eastern Ediacaran–Ordovician Araçuaí orogen (Figs. 1d and 2). The southern section of this region contains features of a passive margin in different stages, represented by (i) the elevated plateau of the Mantiqueira Range in the south, (ii) an intermediate elevation area characterised by an inselberg landscape more towards the north, and (iii) the low-elevation landscape of the Doce River valley in between those highlands (Fig. 3). Within the debate of passive margin evolution, questions can be raised on the post-break-up tectonic evolution of this complex region which basement is largely dominated by the outstanding lithotectonic inheritance left by the Araçuaí orogen.

An ideal tool to investigate passive margin evolution has been found in low-temperature thermochronology (Gallagher and Brown, 1997), such as apatite fission track (AFT) and apatite (U–Th)/He (AHe) thermochronology. These thermochronometers are sensitive to changes within the upper crust (~1–5 km), and are further especially useful to asses basement reactivation (e.g. Gallagher and Brown, 1997; Harman et al., 1998). If well applied, these tools provide means to constrain time, amounts and rates of denudation and have become indispensable to explain geomorphological features of landscapes. Green and Duddy (2018) have recently intensified the debate on the applicability of the AHe method and have shown that interpretations on geological history inferred from AHe data should be treated with the necessary prudence.

In this study we provide new data from AFT and AHe thermochronology from the Araçuaí orogen area of the south-eastern Brazilian highlands and passive margin. Our goal is to use these data to provide a new set of spatial-temporal constraints for the thermo-tectonic evolution and related surface processes of this region, supported by inverse models for the time-temperature paths. We further formulate an hypothesis on the geodynamic context and driving forces for this evolution since break-up.

2. Geological background and regional geomorphology

2.1. Precambrian to early Paleozoic basement

The Araçuaí orogen is the northern part of the Mantiqueira tectonic province, situated in east Brazil (Figs. 1 and 3) (Almeida, 1977; Heilbron et al., 2004). To the east the Araçuaí orogen borders the South Atlantic and to the south, it continues into the Ribeira Belt (Fig. 1d), as the main structural trend diverts from NNE to NE. The southern border is arbitrarily defined at 21°S, bounded by the meridional limit of the São Francisco Craton (SFC; Fig. 1) (Alkmim et al., 2006). The Araçuaí orogen and the West Congo Belt formed the Araçuaí–West Congo orogenic system (AWCO; Fig. 1a–c) that evolved into a unique geodynamic setting related to the Western Gondwana amalgamation during the Ediacaran–Ordovician (Pedrosa-Soares et al., 2001, 2008; Alkmim et al., 2006; Gradim et al., 2014). The unique setting of the AWCO is found in its formation as a confined orogen, bordered by the São Francisco–Congo craton in all directions but the south (Fig. 1a–c) (de Wit et al., 1988; Pedrosa-Soares et al., 2001, 2008; Schmitt et al., 2018).

The basement of the AWCO comprises several metamorphic complexes, including Archean blocks and Rhyacian–Orosirian orogenic systems. Some Archean blocks, e.g. Guanhães and Porteirinha, record orogenic reworking in the Paleoproterozoic and/or Neoproterozoic (Pereira Cruz et al., 2016; Silva et al., 2016; Aguilar et al., 2017; Alkmim and Teixeira, 2017; Teixeira et al., 2017; Degler et al., 2018). One of those metamorphic complexes is the granulitic Juiz de Fora Complex (Fig. 2) (Noce et al., 2007; Fonte-Boa et al., 2017), that was formed as a response to the Rhyacian–Orosirian event (Noce et al., 2007; Heilbron et al., 2010; Degler et al., 2018). The precursor basin of the AWCO emerged in the southern portion of the SFC craton (Fig. 1b and c), as a result of a series of rifting events. The evolution of the AWCO involves three major stages, which are responsible for the emergence of five granitic supersuites from the Early Ediacaran to the Cambrian-Orodovician boundary (Fig. 2) (Pedrosa-Soares et al., 2008). The first, represented by the G1 supersuite of the Rio Doce magmatic arc, characterizes the pre-collisional stage from c. 630 Ma to c. 585 Ma (Novo et al., 2018). The collisional stage is represented by garnet-bearing granites of the G2 supersuite (585–565 Ma). The last stage mostly includes the post-collisional intrusions of the G4 and G5 supersuites (530–480 Ma). The last phase is attributed to the gravitational collapse of the Araçuaí orogenic edifice. The volcano-sedimentary cover of the Rio Doce volcanic arc is represented by the Rio Doce Group, and the back-arc basin fill by the gneissic Nova Venécia Complex (Fig. 2) (Pedrosa-Soares et al., 2008; Gradim et al., 2014).

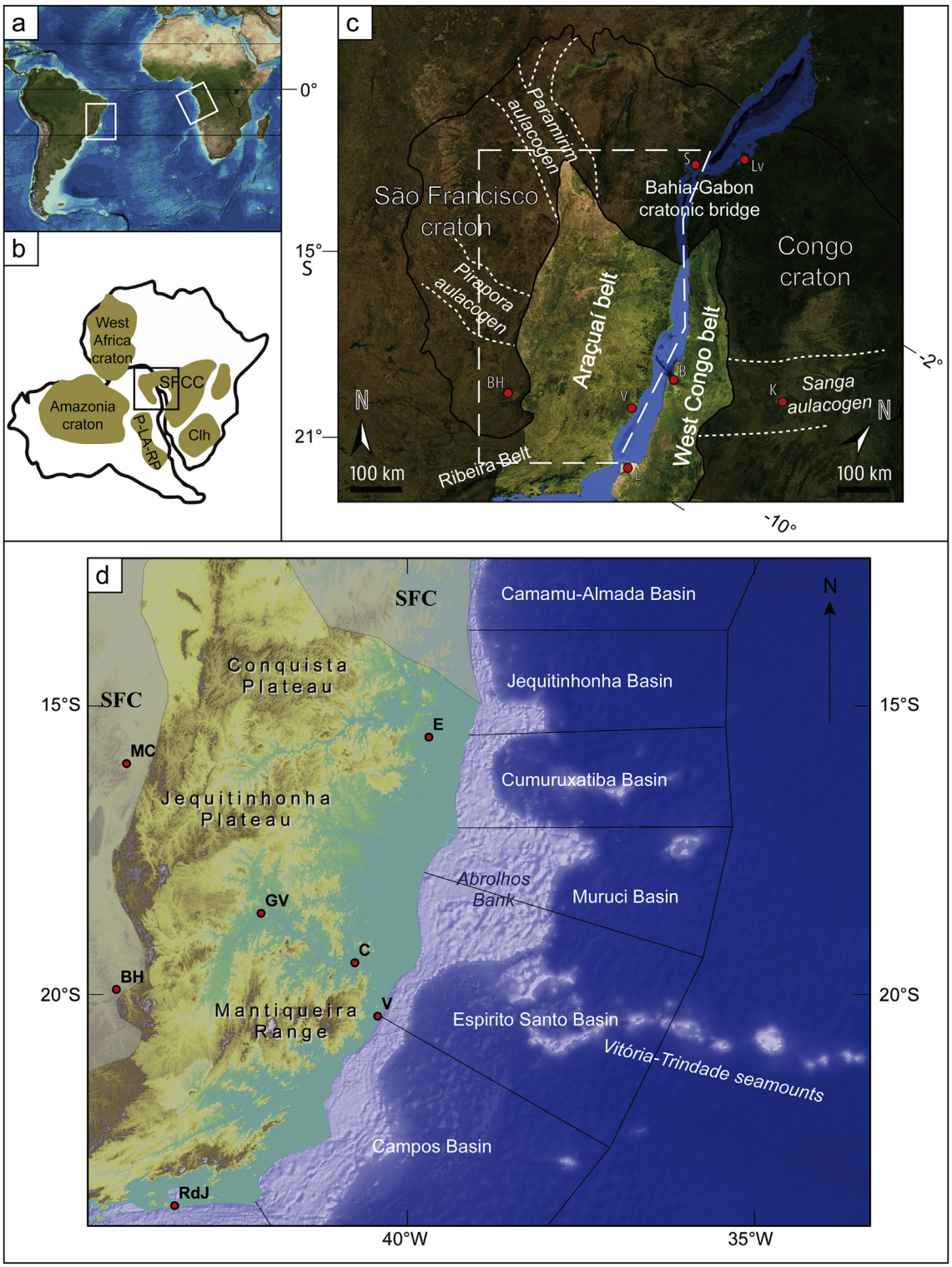

Fig. 1. General overview of the study area. (a) Current setting of the Araçuaí–West Congo orogen (AWCO) (Map of GEBCO, www.gebco.com). (b,c) Neoproterozoic setting of the AWCO (Alkmim et al., 2006; Pedrosa-Soares et al., 2007). (d) Physical overview of the south-eastern Brazilian highlands underlain by the Araçuaí belt, and adjacent basins (NASA SRTM, GEBCO_2014; www.gebco.net). Reference cities: B: Boma, BH: Belo Horizonte, C: Colatina, E: Eunapolis, GV: Governador Valadáres, K: Kinshasa, L: Luanda, Lv: Libreville, MC: Montes Claros, Rdj: Rio de Janeiro, S: Salvador, V: Vitória.

The Colatina Fracture Zone (CFZ) is a ~250 km long group of lineaments oriented in NW–SE direction, cross-cutting the NNE–SSW structural trend of the Araçuaí belt (Fig. 3) (Belém, 2014; Novais et al., 2014). The CFZ served as conduit for mafic dykes, which are dated to the Cambrian (Belém, 2014) and Early Cretaceous (Teixeira and Rodarte, 2003). Probably the CFZ was formed as a result of the Araçuaí orogenic collapse, and was later reactivated during the Early Cretaceous break-up of Gondwana (Mendes, 2017). Another set of structures truncating the Araçuaí structural trend are NW–SE to WNW–ESE lineaments (Fig. 3), such

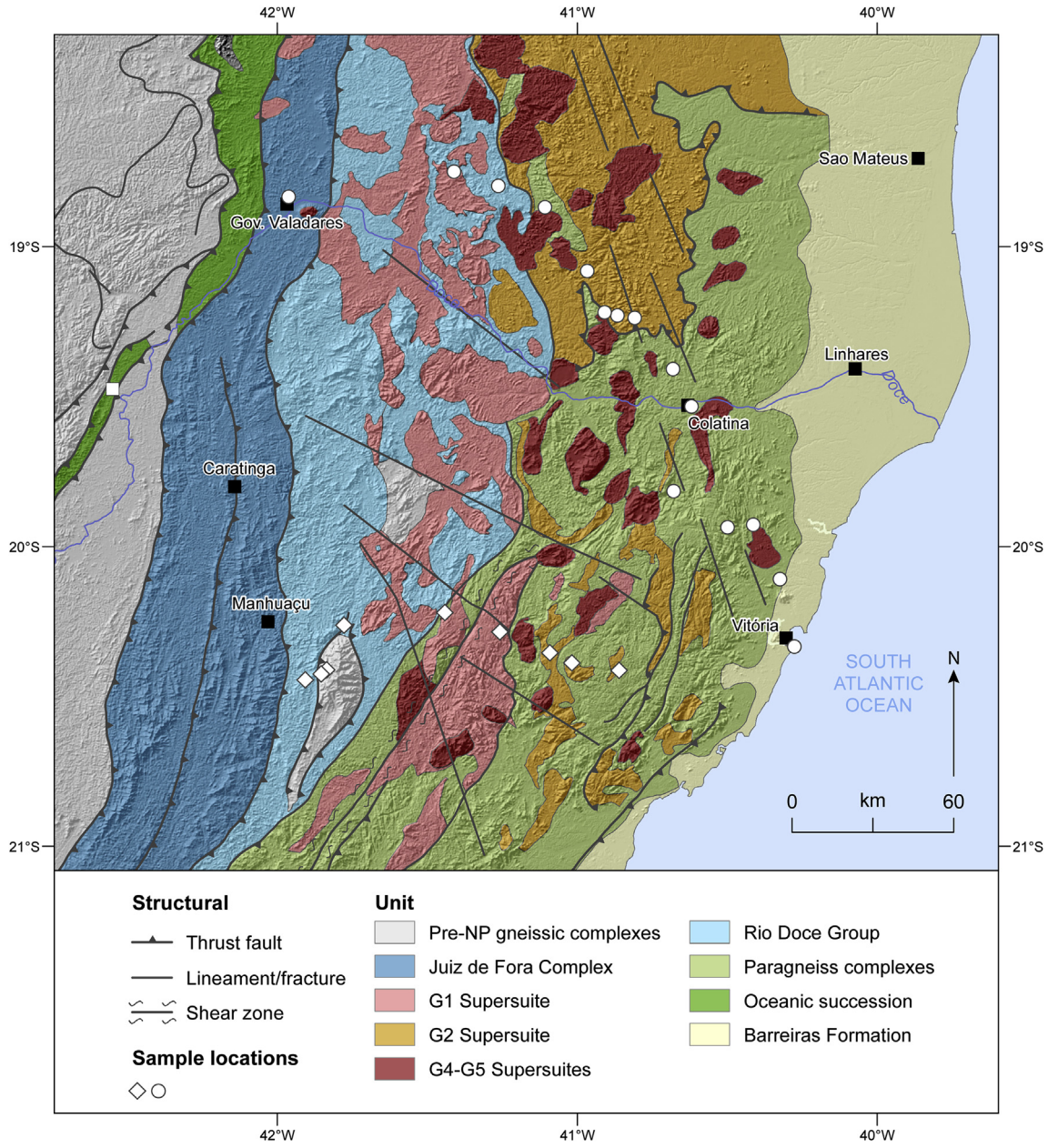

Fig. 2. Geological map of the study area with the main structures and sample locations (after Pedrosa-Soares et al., 2008).

as the Alegre, Piúma and Itaoca lineaments (Calegari et al., 2016; Lourenço et al., 2016; Mendes, 2017). As the Alegre lineament controls both the emplacement of the G5 Supersuite and sedimentation in the Campos basin (Fig. 1d), it is interpreted as Cambrian in age, with important reactivation during the Early Cretaceous and Cenozoic (Calegari et al., 2016; Mendes, 2017).

2.2. Post-break-up evolution

The Ordovician period is followed by a long time interval with relatively few information on the subsequent evolution of the AWCO. As part of the Brasiliano–Pan African network, the area was situated in the continental interior of Gondwana (Scotese, 2004; Schmitt et al., 2018). This continental setting endured until the Mesozoic, when the continent started to stretch to eventually break up, and accommodate the opening of the South Atlantic. With the opening of the South Atlantic between the South American and African continents, the AWCO was separated into two asymmetric counterparts now located in southeast Brazil (the region of the prior Araçuaí orogen) and central–southwest Africa (the region of the prior West Congo Belt) (Fig. 1c).

Perez-Diaz and Eagles (2014) situated the initiation of continental break-up the latest at 138 Ma, with intracontinental deformation mainly taking place in the South American continent until 106 Ma. Ocean spreading propagated from south to north, with an onset around 132 Ma in the far south, coincident with the emplacement of the Paraná–Etendeka flood basalts (Hueck et al., 2018). During this time the South Atlantic margin was subjected to extension and crustal thinning (Torsvik et al., 2009). By ~121 Ma the opening had propagated up to 22°S, just south of the AWCO, and seafloor spreading must have set in between this time and the Aptian/Albian boundary (Torsvik et al., 2009).

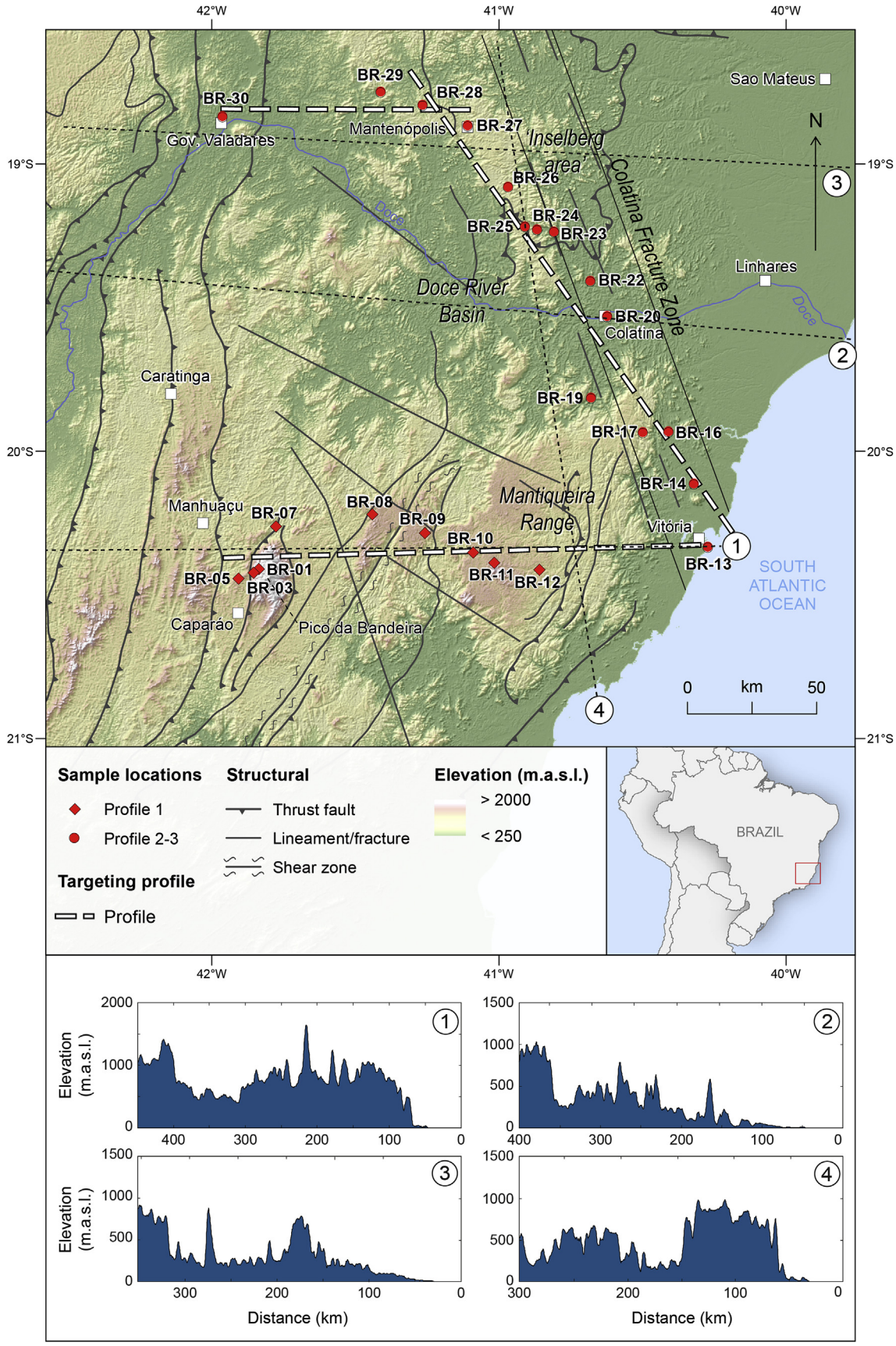

Fig. 3. Map showing sample locations. Background by NASA Shuttle Radar Topography Mission (SRTM) 150 m. Structures adapted from Pedrosa-Soares et al. (2008). Topographic cross-sections of the main landscape types are provided (short dashed line).

The evolutionary stages from rift to drift in the south-eastern Brazilian highlands are recorded in the adjacent Campos and Espirito Santo basins (Fig. 1d) (Mohriak et al., 2008). The sedimentary succession in the basins is subdivided into five phases: the (i) pre-rift (Upper Jurassic–Lower Cretaceous), (ii) syn-rift (upper Berriasian–lower Aptian), (iii) transitional (Aptian), (iv) transgressive drift (upper Albian–lower Eocene), and (v) regressive drift phases (lower Eocene–recent) (França et al., 2007). The pre-rift phase is clearly fault-controlled and produced fluvial-lacustrine sediments directly on top of the basement (Ojeda, 1982; França et al., 2007). During this first stage, erosion products of the Araçuaí belt were identified to be transferred north, to the pre-rift Almada and Camamu basins (Fig. 1d) (Bertotti et al., 2014). The syn-rift stage in the Espirito Santo Basin (Fig. 1d) is characterised by a phase of strong tectonic subsidence (Ojeda, 1982; França et al., 2007). This stage ended with an angular unconformity and transferred to the transitional phase, marked by thick packages of Aptian evaporites (Burke and Sengör, 1988; Torsvik et al., 2009). The transgressive drift phase contains fully marine strata, including carbonate platforms covered by turbiditic deposits (Chang et al., 1992; Mohriak, 2003; Alves et al., 2009). Salt tectonics since the Albian was mainly triggered through gravitational gliding and differential loading (Demercian et al., 1993; Fiduk et al., 2004). During the regressive phase, onshore sediments were transported downslope through canyons and channels (Bruhn and Walker, 1997; Qin et al., 2016). The transition between the two drift phases also coincides with the initiation of a global drop in eustatic sea level (Miller et al., 2005, 2011; Haq, 2014).

Part of the post-break-up history can also be found in the onshore Barreiras Formation, which can be traced along the Brazilian coast (Fig. 2), where it forms the tableland landscape. The formation is found to contain texturally immature detrital material, which was deposited in a coastal/transitional environment (Lima et al., 2006; Rossetti and Domingues, 2012). It was deposited during the early to middle Miocene during high sea level, related to the Mid Miocene Climate Optimum (Zachos et al., 2001; Rossetti and Domingues, 2012).

A remarkable feature offshore, in the north of the Espirito Santo Basin, is the Abrolhos Bank (Fig. 1d), which is argued to be related to the Trindade plume (Cordani, 1970; Thompson et al., 1998). Through drifting of the South American plate, the plume passed under the SFC and Araçuaí belt between ~85 Ma and 55 Ma (Thompson et al., 1998). Due to the extensive thickness of the craton, the plume head is presumed to have spread and stalled under the lithosphere, without resulting magmatism in this area at this time (Thompson et al., 1998). The plume entered the oceanic domain around 55 Ma (Thompson et al., 1998). The thinner oceanic lithosphere could hence explain the episodic magmatism in the base of the regressive drift phase in the Espirito Santo Basin, the development of the Abrolhos Bank, and local tectonic reactivation (Cordani, 1970; Demercian et al., 1993; Thompson et al., 1998). The further apparent drift of the plume can be traced along the Vitória–Trindade sea mount chain (Fig. 1d). It must be noted that there are other views on the origin of alkaline magmatism along the southeastern Brazilian margin (e.g. Almeida, 1991; Ernesto et al., 2002), negating the existence of the Trindade plume. Consequently, we will hereafter refer to the origin of the magmatism with the more generalised term 'Trindade thermal anomaly'.

2.3. Geomorphological context

Following Cohen et al. (2014), the area occupied by the southern section of the former Araçuaí orogen (Fig. 1) is characterised by four geomorphological units: (i) the mountainous area, which is underlain by Proterozoic basement (Fig. 2), showing a multidirectional, rectangular dendritic drainage network; (ii) the coastal tableland formed by the Barreiras Formation (Fig. 2); (iii) the coastal plain, with fluvial to shallow marine Quaternary deposits (Martin and Suguio, 1992); and (iv) the inner continental shelf area (Asmus et al., 1971). The south of the area is characterised by the Mantiqueira Range (Fig. 1d), a high level (~2000 m), low-relief plateau, crosscut by deeply incised valleys (Fig. 3). At the coast, the plateau contains a relatively steep escarpment, as is illustrated in Profile 1 (Fig. 3). Especially the easternmost unit stands out the most, with a clear plateau and escarpments to the south, to the coast in the east and to the Doce River basin in the north. The Mantiqueira Range is developed along the Neoproterozoic NNW–SSE trend, and thus also quasi parallel to the coastline (Figs. 1d and 3). It does however not show a coincidence with lithological contrasts (Fig. 2). Assuming similarity with the northeast Brazilian margin, this plateau was formed as an uplifted peneplain (Peulvast et al., 2008; Japsen et al., 2012a; Jelinek et al., 2014).

The area north of the Doce River basin is famous for its granitic inselbergs, locally known as *pão de açúcar* or sugar loaf mountains (Fig. 3). The density of these geomorphologic features is high, with the inselbergs in different stages of exhumation (Owen, 2014). The granites are crosscut by the CFZ, which plays a major role in the emergence of the inselberg landscape (Owen, 2014). Weathering propagates along the joints and preshapes the proto-landscape below-surface. Later uplift and denudation preferentially removes the weathered material from the joints-network, and exfoliation erosion finally results in the characteristic inselbergs (Chicarino Varajão and Alkmim, 2015 and references therein). In the 'inselberg area' (Fig. 3), the different states of inselberg morphologies are attributed to differential denudation along the reactivated Neoproterozoic shear zones (Chicarino Varajão and Alkmim, 2015).

The Mantiqueira Range (Fig. 3) forms the watershed of the Doce River, one of the largest rivers of eastern Brazil (Oliveira and Quaresma, 2017). Its fluvial sediments are mainly transported from the river's catchment area to the Espirito Santo Basin (Fig. 1d). The denudational capacity of the Doce River basin is relatively high since its great altimetric amplitude and its direct link to the ocean base level (Marent et al., 2018). The drainage pattern of the Doce River and tributaries is largely influenced by the local structural trends (Cohen et al., 2014). The Doce River follows the Neoproterozoic NNE–SSW trend to the north, through the Doce River graben (Cherem et al., 2012), past the Mantiqueira Range, and then changes direction towards the east, cross-cutting the main structural trend to its mouth.

2.4. Existing thermochronology data

The thermochronology of east Brazil's passive margin has already been the focus of many studies. Research has been conducted, mainly using the apatite (AFT) and/or apatite (U–Th)/He (AHe) methods, in south-eastern Brazil (Gallagher et al., 1994, 1995; Tello Saenz et al., 2003, 2005; Franco-Magalhães et al., 2010; Cogné et al., 2011, 2012; Karl et al., 2013; Engelmann de Oliveira et al., 2016a, b), northeast Brazil (Harman et al., 1998; Turner et al., 2008; Morais Neto et al., 2009; Japsen et al., 2012a; Jelinek et al., 2014) and central east Brazil (Jelinek et al., 2014). These studies identified episodes of uplift and exhumation during the Permian–Early Triassic (Jelinek et al., 2014), Triassic–Jurassic (Japsen et al., 2012a; Karl et al., 2013), Early Cretaceous (Cogné et al., 2011; Japsen et al., 2012a; Jelinek et al., 2014), and Late Cretaceous (Cogné et al., 2011, 2012; Japsen et al., 2012a; Karl et al., 2013; Jelinek et al., 2014). They also report scattered Cenozoic cooling.

Often ages or basement cooling events (interpreted as basement exhumation) inferred from numerical modelling differ strongly between regions. This can be attributed to spatial differences, such as the presence of structural blocks (Karl et al., 2013), geomorphological differences (Jelinek et al., 2014) or geological setting along the large and diverse area set by the Brazilian passive margin.

3. Materials and methods

3.1. Samples and sampling strategy

For this study we acquired a total of 29 samples concentrated around three profiles (Fig. 3), two of which in E–W direction, perpendicular to the main structural trend (SSW–NNE), and one in SE–NW direction. All samples are from the Paleoproterozoic crystalline basement or Neoproterozoic to Ordovician granitic and gneissic complexes of the Araçuaí orogen (Fig. 2). Main lithologies include high-grade metamorphic or granitoid rocks. Details on sample location, lithology and analyses are listed in Table 1.

Profile 1 (Fig. 3) lies in the southernmost portion of the study area and follows a W–E direction, between Caparáo ridge and the coast (Vitória). The profile is mainly situated on the elevated plateau of the Mantiqueira Range and crosses several shear zones. It contains a vertical section (BR-01–05) on the Pico da Bandeira (2892 m.a.s.l.; Fig. 3), covering 971 m of elevation difference. The relief along this profile clearly shows the escarpment to the coastal plain (Fig. 3). Profile 3 (Fig. 3) follows a W–E direction from Governador Valadáres to Mantenópolis, where it continues into Profile 2 (Fig. 3), which runs SE–NW to Vitória. Profiles 2–3 lies north of the Mantiqueira Range at lower altitudes than Profile 1. Samples from along Profiles 2–3 are from the Doce River basin, the lower elevated range with high inselberg density, and the coastal plain. The profile runs along and across the Colatina Fracture Zone (Fig. 3). North of Colatina the profile contains a second vertical section, with one sample (BR-24) from the top of an inselberg mountain. We aimed at a sample spacing of 10–20 km, in order to register spatial differences in the thermochronology signal. These criteria were not always met, due to lack of outcrops, adequate basement lithology or apatite yield.

Apatite crystals were separated using conventional techniques. After separation, samples were inspected for apatite yield and quality. Four samples were discarded due to insufficient apatite of adequate quality.

3.2. Analytical procedure

For this study we combined two low-temperature thermochronology techniques, the apatite fission track (AFT) and apatite (U–Th)/He (AHe) methods. The AFT method was applied to all samples and AHe was applied to all suitable samples (Appendix A; Table 1). The combination of two thermochronometers could provide stronger and more detailed information on the sample's cooling history. Fission tracks in apatite are considered stable on geological time scales at temperatures below ~60 °C and anneal rapidly if they are heated over ~120 °C (Wagner and Van den haute, 1992). They reduce to shorter lengths through partial annealing in the temperature window between ~60 °C and ~120 °C, i.e. the apatite partial annealing zone (APAZ) (Gleadow and Duddy, 1981; Gleadow et al., 1986a; Green et al., 1986). The annealing is partly influenced by the apatite chemical composition (Carlson et al., 1999; Barbarand et al., 2003a). From the areal density of surface fission tracks we can thus infer the age when a sample cooled through the ~100 °C isotherm (Wagner and Van den haute, 1992). Besides the time of cooling, also the track length-frequency distribution of confined tracks, i.e. tracks that do not crosscut the polished surface and thus retain their entire etched length, provides us with information on the thermal history a sample experienced (Gleadow et al., 1986b), such as the rate and complexity of cooling. Note that (re)heating will cause shortening of the tracks, causing a broadening of the length-frequency distribution and a resulting mixed age (Wagner and Van den haute, 1992).

The apatite (U–Th)/He method finds its principles in the balance between the production of ^{4}He by alpha decay and the loss of He due to thermal diffusion (Zeitler et al., 1987; Meesters and Dunai, 2002). An estimated closure temperature of ~50–70 °C was found for a system with a grain size between 50 μm and 100 μm that cooled at a rate of 1–10 °C/Ma (Farley, 2000). In theory these lower closure temperatures would make AHe better suited to constrain changes in the cooler uppermost crust as compared to AFT. However, reported AHe data often show excess dispersion

Table 1
Location, lithology and applied method details from samples analysed in this study. X: longitude, Y: latitude, Z: elevation in meters above sea level, D: distance to coast, AFT: apatite fission track analysis, AHe: apatite (U–Th)/He dating. Coordinates are in WGS84.

Sample	X (°W)	Y (°S)	Z (m.a.s.l.)	D (km)	Group	Lithology	Method
BR-01	41.8366	20.4106	1985	130.65	Juiz de Fora Cplx	Granulite	AFT[a]
BR-03	41.8546	20.4226	1215	131.64	Juiz de Fora Cplx	Granulite	AFT-AHe
BR-05	41.9078	20.4437	1014	135.26	Juiz de Fora Cplx	Tonalite	AFT-AHe
BR-07	41.7770	20.2614	520	133.66	G1 Supersuite	Granodiorite	AFT-AHe
BR-08	41.4419	20.2183	955	105.83	G1 Supersuite	Paragneiss	AFT
BR-09	41.2583	20.2840	1086	85.57	G1 Supersuite	Granodiorite	AFT-AHe
BR-10	41.0911	20.3521	949	66.66	G2 supersuite	Granodiorite	AFT-AHe
BR-11	41.0174	20.3873	1112	58.04	G5 Supersuite	(Monzo) Granite	AFT
BR-12	40.8597	20.4123	818	42.40	G5 Supersuite	Granite	AFT
BR-13	40.2731	20.3339	1	0.00	G5 Supersuite	Granite	AFT-AHe
BR-14	40.3215	20.1138	37	10.33	G5 Supersuite	Charnockite	AFT-AHe
BR-16	40.4096	19.9324	59	28.40	Nova Venécia Cplx	Paragneiss	AFT-AHe
BR-17	40.4989	19.9352	415	36.34	G5 Supersuite	Charnockite	AFT-AHe
BR-19	40.6787	19.8146	141	59.35	Nova Venécia Cplx	Paragneiss	AFT-AHe
BR-20	40.6223	19.5311	49	70.11	Nova Venécia Cplx	Paragneiss	AFT
BR-22	40.6809	19.4084	62	78.56	Nova Venécia Cplx	Paragneiss	AFT
BR-23	40.8080	19.2362	115	95.52	G2 Supersuite	Foliated granite	AFT-AHe
BR-24	40.8664	19.2295	736	101.69	G2 Supersuite	Foliated granite	AFT[b]
BR-25	40.9089	19.2184	437	106.31	G2 Supersuite	Foliated granite	AFT[b]-AHe
BR-26	40.9669	19.0807	485	115.41	G2 Supersuite	Foliated granite	AFT[b]
BR-27	41.1081	18.8674	604	134.82	S2 Supersuite	Foliated granite	AFT-AHe
BR-28	41.2654	18.7963	329	152.68	G2 Supersuite	Granite	AFT[b]-AHe
BR-29	41.4108	18.7506	351	168.72	G1 supersuite	Tonalite	AFT-AHe
BR-30	41.9624	18.8355	188	223.62	Juiz de Fora Cplx	Granite	AFT[b]-AHe

[a] No length measurements.
[b] Treated with heavy ion bombardment to enhance confined AFT density.

(Fitzgerald et al., 2006; Danišík et al., 2008), and/or ages older than the AFT age (e.g. Belton et al., 2004; Hendriks and Redfield, 2006; Feinstein et al., 2009; Wildman et al., 2016). The observation of AHe ages becoming progressively older with older AFT age, led Green et al. (2006) and Shuster et al. (2006) to the conclusion that radiation damage of the crystal lattice causes enhanced He retention. In these cases, the aforementioned closure temperature would overestimate true He-diffusion. Our present understanding of the accumulation and annealing of radiation damage accumulation is based on the AFT system. AFT annealing models explicitly take into account the chemical composition of the analysed grains, and AHe models should therefore do the same (Gautheron et al., 2013). Unfortunately, compositional information is rarely acquired during AHe data acquisition. This may be one of the reasons why current models for AHe data interpretation (e.g. Flowers et al., 2006) often fail to explain most of the age dispersion (Green and Duddy, 2018).

Both AFT and AHe methods in principle thus form an ideal instrument to detect thermal events of the upper crust, such as exhumation and denudation and related landscape evolution (Reiners and Shuster, 2009; Sobel and Seward, 2010; Glorie et al., 2012; Brown et al., 2013; Glotzbach et al., 2015). Moreover, through inverse modelling with this thermochronologic data it is possible to reconstruct basement time-temperature (t-T) paths (Ketcham et al., 1999, 2007a; Gallagher, 2012).

Our procedure is based on the standard procedure of the fission track laboratory at Ghent University (De Grave and Van den haute, 2002; Glorie et al., 2010; Nachtergaele et al., 2018), however contains some analytical adaptations described in Appendix A.

All samples in this study were etched in a 5.5 mol/L nitric acid solution at 21 °C, for 20 s (Donelick, 1993). We dated the samples using the external detector method (EDM) (Hurford and Green, 1982; Jonckheere, 2003a) and ages were calculated and reported following the conventional ζ approach (Hurford and Green, 1983; Hurford, 1990). All analyses were performed by one analyst ($\zeta = 283.84 \pm 4.30$ yr cm^2, based on Fish Canyon Tuff and Durango age standards and the IRMM-540 dosimeter glass; Appendix A). We aimed at a total of 1000 spontaneous tracks (~3% error) for surface track density assessment and the measurement of 100 confined tracks for the construction of the length-frequency distribution. For each confined track the angle to the crystallographic c-axis was also measured to quantify annealing anisotropy (Barbarand et al., 2003b; Ketcham et al., 2007b). Since the ease/possibility to find this number of tracks strongly depends on the spontaneous track density, a second mount was made for each sample. A subset of these second mounts was subjected to heavy ion bombardment (HIB) to generate a higher number of confined tracks (Table 1; Appendix A) (Jonckheere et al., 2007) at GSI Helmholtz (Germany). Central ages and according sample dispersion (Galbraith and Laslett, 1993; Galbraith, 2005) are reported and a χ^2 homogeneity test (Green, 1981; Galbraith, 2005) was performed for each sample. We measured D_{par} (Donelick, 1993) as a proxy for chemical composition to account for compositional-related differences in annealing kinetics.

Based on sample quality a subset of samples was selected for AHe analysis, which was performed at the Geochronology Centre at University College London. In an effort to limit dispersion, we aimed at only selecting whole, quasi-euhedral, transparent, clean grains without inclusions, following the recommendations of Flowers and Kelley (2011). For each sample 10–15 grains were packed as separate aliquots in Pt capsules and degassed using laser-heating (House et al., 2000). To characterise the diffusion domain and for alpha ejection correction, we measured three axes of grain dimensions under a normal light microscope. After degassing, the grains were dissolved in 65% HNO_3 and the main alpha emitters (U and Th) were measured using an ICP-MS system. Outliers were detected following the modified Chauvenet criterion embedded in IsoplotR (Vermeesch, 2018). Single aliquot ages were calculated using HelioCalc (http://www.ucl.ac.uk/~ucfbpve/heliocalc/) and central ages and dispersion were calculated in IsoplotR (Vermeesch, 2008, 2018). Raw ages were plotted against equivalent uranium ($eU = U + 0.235Th$) and effective spherical radius (R^*; Farley, 2002; Meesters and Dunai, 2002) to investigate internal correlations.

Samples that passed the χ^2 test for AFT, and which yielded sufficient (>70) confined track length measurements were withheld for Markov Chain Monte Carlo inverse modelling, implemented in QTQt (Appendix A; Gallagher et al., 2009; Gallagher,

Table 2
Summary of AHe and AFT results, with Z: elevation in meters above sea level, D: distance to coast, s.e.: standard error, MTL: mean track length, n.m.: no measurements. All reported ages are central ages.

Sample	Z (m.a.s.l.)	D (km)	AHe age (Ma)	Dispersion (%)	AFT age (Ma)	s.e.	MTL (μm)	St. dev. (μm)
BR-01	1985	130.7	n.m.	n.m.	145.3	32.8	n.m.	n.m.
BR-03	1215	131.6	62.1	11.6	83.9	4.8	13.2	1.5
BR-05	1014	135.3	76.8	15.0	63.6	2.3	13.0	1.5
BR-07	520	133.7	70.8	0.0	63.1	2.5	13.0	1.3
BR-08	955	105.8	n.m.	n.m.	76.8	3.5	13.2	1.5
BR-09	1086	85.6	100.1	16.0	71.0	2.7	13.0	1.3
BR-10	949	66.7	85.4	27.0	61.8	2.5	13.1	1.1
BR-11	1112	58.0	n.m.	n.m.	68.2	2.7	13.1	1.4
BR-12	818	42.4	n.m.	n.m.	61.7	3.4	13.7	0.7
BR-13	1	6.3	57.3	13.6	80.9	4.5	13.5	1.1
BR-14	37	10.3	60.1	13.6	81.3	3.5	13.6	1.2
BR-16	59	28.4	71.9	15.4	71.7	2.1	13.1	1.2
BR-17	415	36.3	77.7	8.6	78.8	4.1	13.5	1.3
BR-19	141	59.4	59.1	10.6	73.1	3.5	13.1	1.2
BR-20	49	70.1	n.m.	n.m.	63.7	5.6	12.2	1.8
BR-22	62	78.6	n.m.	n.m.	78.2	3.2	13.0	1.5
BR-23	115	95.5	87.5	9.3	78.1	3.5	12.8	1.5
BR-24	736	101.7	n.m.	n.m.	89.9	5.5	12.7	1.6
BR-25	437	106.3	74.0	56.0	80.6	3.9	13.0	1.5
BR-26	485	115.4	n.m.	n.m.	80.9	3.1	13.2	1.3
BR-27	604	134.8	91.5	12.2	67.2	2.1	12.8	1.3
BR-28	329	152.7	88.7	15.4	88.4	4.0	13.0	1.3
BR-29	351	168.7	71.0	6.6	83.6	3.8	12.6	1.7
BR-30	188	223.6	58.2	17.8	70.4	4.5	13.0	1.2

2012). The prior was set to the (oldest age ± oldest age), as is standard in QTQt. This choice was made based on a potential prior-age relation, for which a constant prior for all samples (with different ages) might influence the output t-T paths, resulting in easier cooling histories for younger AFT ages. We used the annealing model of Ketcham et al. (2007a), with D_{par} as the kinetic parameter. Because of the irreproducibility of some AHe datasets (Green and Duddy, 2018), we calculated expected t-T paths for the AFT data only (Set 1). The AFT data were only augmented with the AHe data if a (weak) correlation between raw AHe age and both eU and R^* could be found and where dispersion was smaller than 20% (Set 2). Inversion with AHe was corrected using the RDAAM model (Flowers et al., 2009). Models were only withheld if the predicted age falls within uncertainty of the observed age. Joint or simultaneous modelling of samples from one block, with different elevations, results in models with a higher geological confidence. Adjacent samples with a logical age-elevation relationship, i.e. ages becoming older with elevation, were modelled together. When good search parameters were found, the model was run for $1E^6$ burn-in and $2E^5$ post-burn in iterations.

4. Results

We present new AFT data from 24 samples, of which 23 including length measurements, and AHe data from 16 samples. A summary of the results can be found in Table 2. An overview of the spatial distribution of AFT ages is shown in Fig. 4. Full data tables and figures are to be found in Appendix A.

4.1. Results from AFT analysis

For most samples, more than 1000 spontaneous tracks were counted (Appendix A, Table B.1). All samples, except BR-20, pass the χ^2 test. BR-01 is imprecise (22% error) due to its low ($5.5E^4$ cm^{-2})

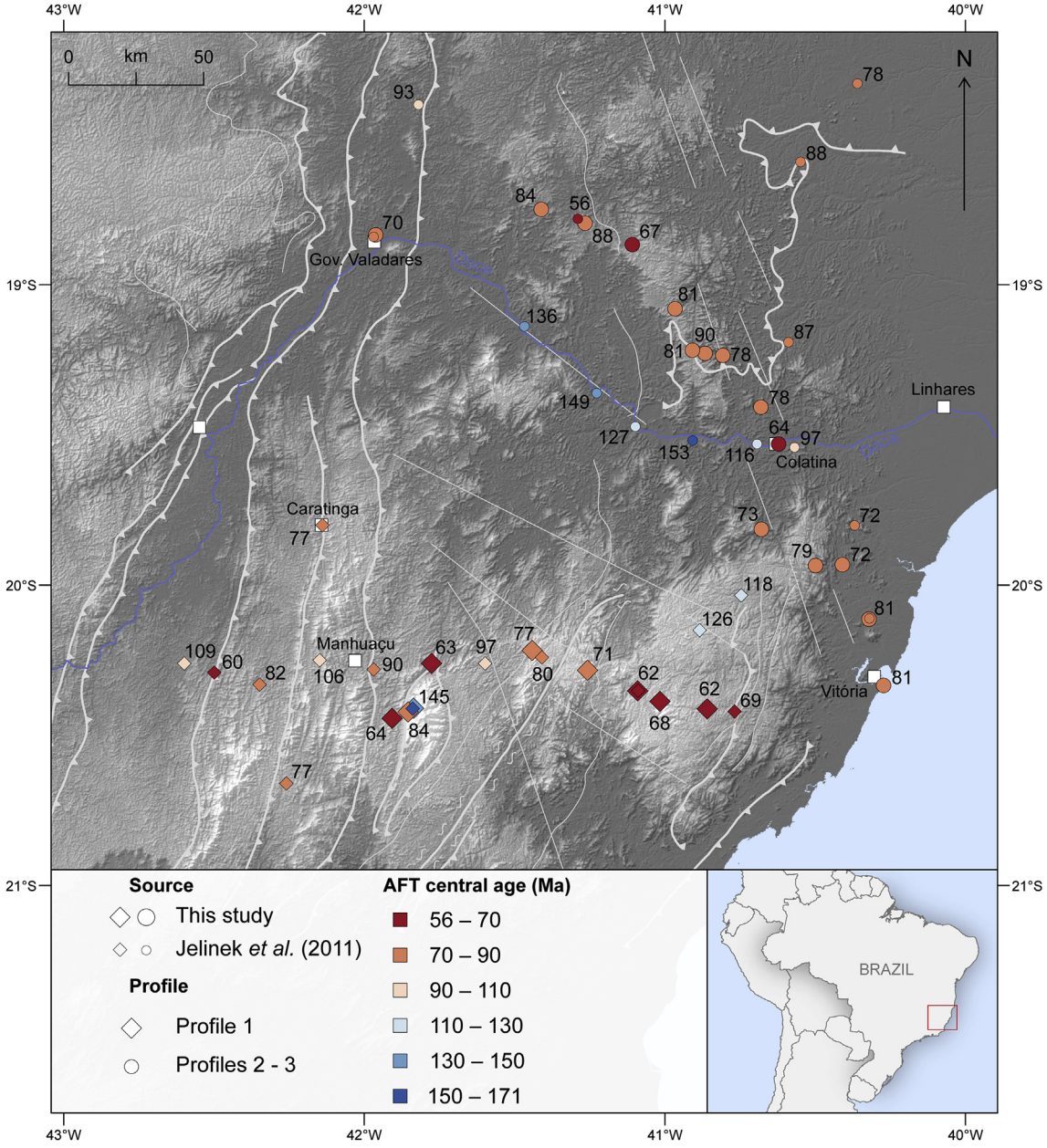

Fig. 4. Map showing AFT central ages, including results from Jelinek et al. (2014). Structures adapted from Pedrosa-Soares et al. (2008). Background by NASA SRTM 150 m.

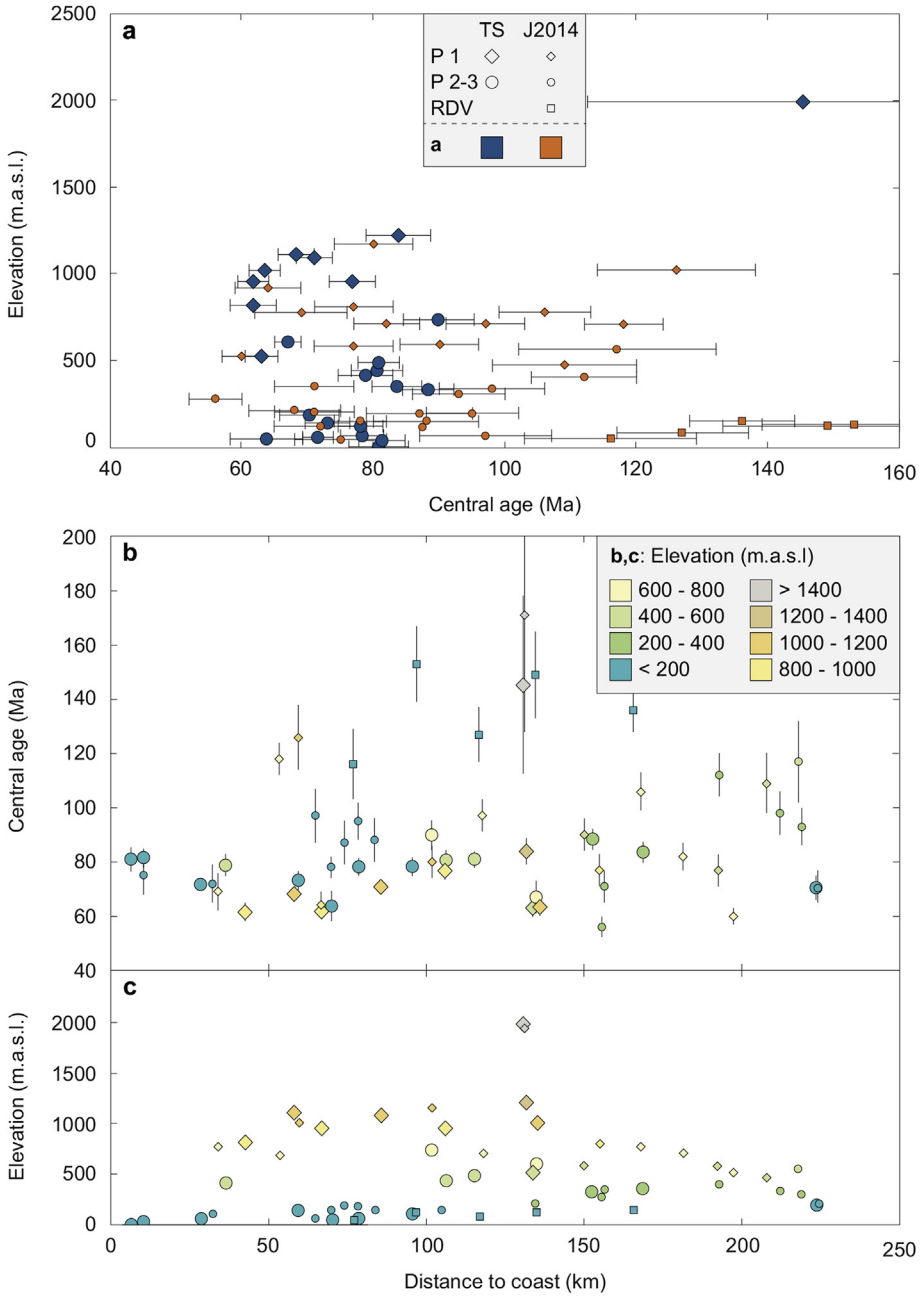

Fig. 5. (a) Age-elevation plot. P1: Profile 1, P2-3: Profiles 2–3, RDV: Doce River Valley, TS: this study, J2014: Jelinek et al. (2014). (b) Distance to coast – central age. (c) Distance to coast – elevation plots. Colour-coding according to elevation.

track density and its low uranium content. All ages are significantly younger than the Brasiliano–Pan African (Neoproterozoic–Ordovician) event and younger than the West-Gondwana break-up (Early Cretaceous), as the AFT central ages of all samples, except BR-01, are Late Cretaceous to early Paleogene (60–90 Ma) (Table 2). Only sample BR-01, which in fact is from the highest elevation, gives a poorly constrained Early Cretaceous age of about 145 ± 33 Ma (Table 2).

The majority of the analysed samples come from elevations lower than 1250 m.a.s.l., with only BR-01 originating from an altitude of 2000 m.a.s.l. (Fig. 3). On the age-elevation plot (Fig. 5a) all samples scatter significantly and do not show a clear correlation. The samples from Profile 1 (Fig. 3), which are mainly from the elevated plateau of the Mantiqueira Range, can be distinctly separated from the samples from Profiles 2–3, which come from lower elevations (Fig. 5a). The Mantiqueira Range samples seem to roughly describe a normal trend of higher age with elevation (Fig. 5a). The same holds true for the samples of the coastal plain and north of the Mantiqueira Range. Sample BR-17, which is from a valley incised in the elevated plateau, plots within the age-elevation group of Profiles 2–3 (Fig. 5a). BR-13, which is located at the intersection of Profiles 1 and 2 plots within the Profiles 2–3 group. Together with BR-14 it appears older within the trend described by the lower elevation samples. The age-elevation pattern points to a complex, non-uniform thermo-tectonic history for the study area (Fig. 5a).

AFT length data is also displayed in Table 2. Detailed information and length-frequency histograms of each sample are provided in

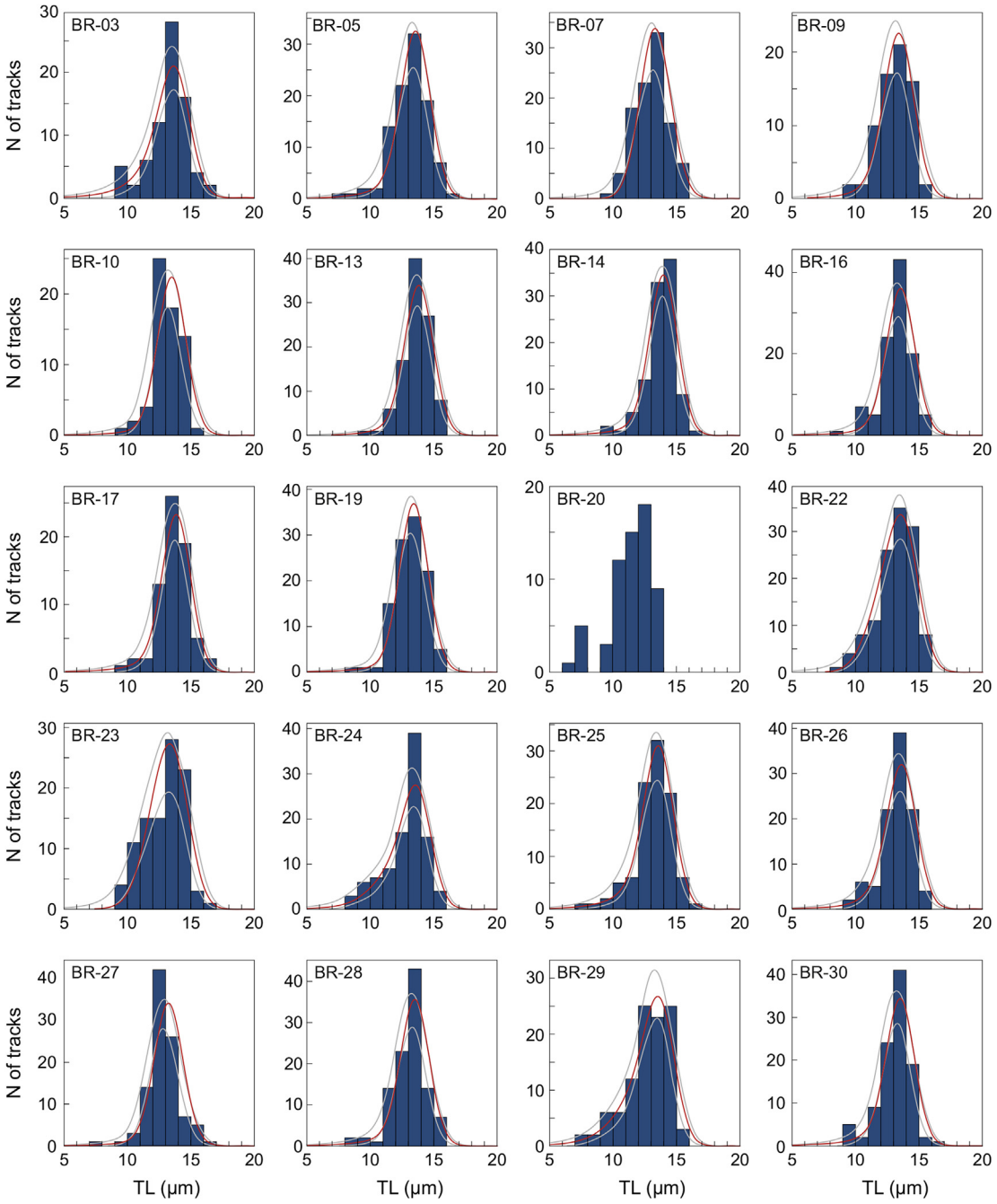

Fig. 6. AFT confined track length-frequency distributions. TL: measured track length. Red and grey curves represent the predicted length distributions and 90% confidence intervals from inverse modelling in QTQt (Gallagher, 2012).

Table B.2 of Appendix A and Fig. 6. Due to its low track density sample BR-01 did not yield sufficient lengths (<10) to display a representative length distribution. Only 23 tracks could be measured in sample BR-12, due to the low number of good quality grains. This low number of tracks does not allow producing a reliable length histogram and we will therefore not include the length distribution of this sample in further discussions. For eight other samples the targeted number of 100 confined tracks was not reached (Appendix A, Table B.2). Nonetheless, enough tracks could be measured to create a representative length-frequency histogram (Fig. 6). Mean track lengths are mostly similar and are overall medium long (12.2–13.6 μm) with a unimodal distribution (Table 2; Fig. 6). Standard deviation is rather narrow, ranging between 0.7 μm and 1.7 μm (Table 2). Standard deviation is also negatively correlated ($R^2 = 0.48$) with mean track length (Appendix A, Fig. B.6), meaning that the distribution becomes wider with shorter mean track length. Skewness is subtly negative for all samples (−0.2 to −1.1: Appendix A, Table B.2), and does not show a correlation with mean track length or standard deviation. BR-14 (13.6 μm), BR-17 (13.5 μm) and BR-13 (13.5 μm) exhibit the longest lengths of our dataset (Table 2). BR-20 (12.2 μm) yields the shortest lengths, followed by BR-29 (12.6 μm) and BR-24 (12.7 μm). All other samples fall within an interval of 13.0 ± 0.2 μm. When plotting the AFT central age versus the mean track length, no clear 'boomerang' trend (Green, 1986) is obtained (Fig. 7), since measured mean lengths only encompass a narrow interval

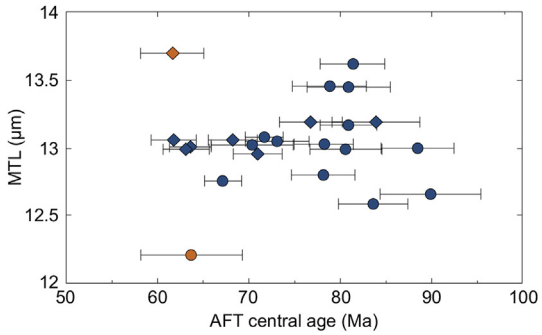

Fig. 7. AFT age – mean track length (MTL) or "boomerang plot". As track lengths are mostly similar, there is no clear trend showing. Disregarded samples BR-12 and BR-20 are marked in orange.

(~1.5 µm). We opted not to apply c-axis projection for reasons mentioned in Appendix A.

The D_{par} values measured vary between 1.4 µm and 1.9 µm (Appendix A, Table B.2), indicating fluorine-rich apatites (Donelick, 1993; Sobel and Seward, 2010).

There is no simple correlation between the AFT central ages and the distance to the coast (Fig. 5b). Potential correlations would furthermore be obscured due to elevation differences. Therefore we colour-coded symbols based on altitude (Fig. 5b and c). From ~45 km inland, AFT ages gradually become older, until ~140 km. The coastal samples, BR-13 and BR-14 are older than expected from the aforementioned trend between 405 km and 140 km. Furthermore, when considering the elevation, the complexity of the spatial pattern of the AFT ages (Fig. 4) becomes more clear, with samples of higher altitude plotting younger or at the same age as samples from lower altitudes. In general, the highest mean track length is from near the coast, gradually becoming shorter inland (Fig. 5b).

4.2. Results from AHe analysis

We analysed 159 single-grain aliquots from 16 samples for AHe (Appendix A, Table B.3). In a first step, a weighted mean for the AHe age was calculated in IsoplotR (Vermeesch, 2018). This module contains the modified Chauvenet criterion (Vermeesch, 2018), which removes outliers that do not fit a Normal distribution with two sources of uncertainty (the analytical uncertainty and geological dispersion). Twenty-nine aliquots were removed from the dataset. Outliers could have been produced by multiple factors, including external (partial crushing of grain after degassing, bad laser-Pt coupling, incomplete dissolution, …) and internal effects, that are reported to produce high degrees of dispersion (e.g. Wildman et al., 2016). As is often the case for AHe results, dispersion is indeed high in our samples, even after removing the outliers, i.e. up to 56% (Table 2). Most samples show dispersion around 10%–30%. BR-07 is the only sample with very small dispersion (after removing six outliers). We calculated the Mean Square of the Weighted Deviates (MSWD) (McIntyre et al., 1966; Vermeesch, 2010) to quantify the degree of dispersion (Appendix A, Table B.3). All samples except BR-07 are overdispersed with respect to the analytical uncertainties ($10 < MSWD < 250$). Commonly cited culprits for this dispersion are high-U submicroscopic inclusions creating parentless He (e.g. Farley and Stockli, 2002), negated by Vermeesch et al. (2007), alpha emitter zonation (e.g. Meesters and Dunai, 2002; Farley et al., 2011; Flowers and Kelley, 2011) or other defects and irregularities (e.g. Gerin et al., 2017; Zeitler et al., 2017; McDannell et al., 2018). As suggested by Flowers and Kelley (2011), information on the probability of these effects can be found in thin sections and polished and etched grains

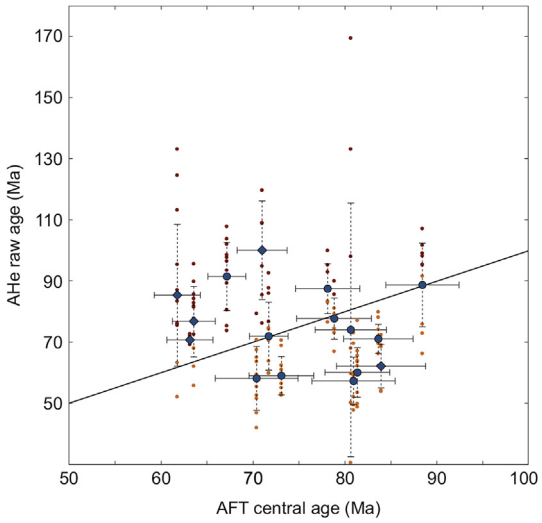

Fig. 8. AHe raw central age vs. AFT central age. AHe single aliquot raw ages are indicated with orange dots for ages younger than the AFT central age and red if older than the AFT central age. Error bars are one standard error for AFT (full line) and dispersion for AHe (dashed line). The 1:1 line where AFT age equals AHe age, is represented by the black line.

and the external detector for AFT analysis. For this paper we provide a qualitative description. From thin sections we did not find evidence for frequent neighbouring U-rich minerals. Larger inclusions that are found in the external detector were also visible within the grains, suggesting that these inclusions would also have been detected while selecting the grains for AHe. It is still possible that small (sub-microscopic) inclusions were overlooked, but volumetric considerations suggest that these are unlikely to have a major effect on the AHe age (Vermeesch et al., 2007). During HNO_3 digestion, these inclusions would not have been dissolved, thus introducing parentless He. Inspection of the grains and the external detectors from AFT analyses revealed that a minority of samples show U-zonation in some grains (Appendix A, Fig. B.6). Uranium-zonation varies between fully homogenous, patches of low/high uranium or growth zonation. The presence of zonation however varies greatly between and within samples. We also found line defects or fluid inclusions in some samples (Appendix A, Fig. B.7). Since the presence of defects, zonation and inclusions varies strongly between grains, this might introduce differences in He-trapping and thus contribute to a higher degree of dispersion. The same anomalies can also obscure age-eU correlations.

AHe central ages are mainly Late Cretaceous and vary between about 57 Ma and 100 Ma (Table 2). When plotting AHe against AFT ages (Fig. 8), they scatter on both sides of the 1:1 line, with some of the AHe ages being older than the AFT ages. All Profile 1 samples, with the exception of BR-03, have an AHe age older than their corresponding AFT age. From Profiles 2–3, only BR-27 and BR-23 show ages older than their AFT age. All other samples display overlapping AFT and AHe ages or AHe ages younger than their AFT central age. We did not find evidence of correlation between AFT and AHe central ages. When plotting AHe central ages against eU and induced track density, the result looks similar, as expected. Age-eU correlation is statistically insignificant (Appendix A, Fig. B.2a; $R^2 = 0.07$). To test for the influence of apatite chemistry, we also plotted against D_{par}, which displays a very weak to negligible negative correlation between AHe age and D_{par} (Appendix A, Fig. B.2b; $R^2 = 0.12$).

None of the samples show a strong internal correlation with neither eU nor R^* (Appendix A, Fig. B.1). Some samples show a

strong positive correlation for R*, but a negative one for eU, while other samples do not exhibit any correlation at all. Age-eU and age-R* correlations are moderate for BR-13, BR-16, BR-17 and BR-28 and weak for BR-27, BR-29 and BR-30. BR-25 has a strong negative correlation with eU, but a strong positive one with R*.

4.3. Results from inversion

All samples that yielded more than 70 confined tracks were withheld for inversion and thermal history modelling. Only samples BR-13, BR-16, BR-17 and BR-28 show correlation with both eU and R*. BR-27, BR-29, BR-30 can also be added, weakly correlated to eU and R* (Appendix A, Fig. B.1). We modelled these samples with both AFT and AHe data, using RDAAM kinetics (Flowers et al., 2009).

Set 1 (only AFT data) results can basically be grouped in three major expected t-T path morphologies. Samples BR-03 and BR-29 show a quasi linear, protracted cooling since *c.* 100 Ma (Appendix A, Fig. B.3). BR-25 and BR-26 show protracted cooling, also since *c.* 100 Ma. Most complex models are displayed by samples BR-22, BR-23 and BR-24. BR-22 and BR-23 show accelerated cooling since *c.* 100 Ma, with stability between 85 Ma and 60 Ma, after which they continue cooling gradually (Appendix A, Fig. B.3). Sample BR-22 shows a similar pattern, although with a lower magnitude of accelerated cooling since *c.* 100 Ma. All other models show one major phase of cooling, between 100 Ma and 70 Ma (Appendix A, Fig. B.3). A minor cooling phase is also displayed since 10–5 Ma for each expected t-T path. The late cooling phase may be explained as a well-known artefact of the annealing models (e.g. Jonckheere, 2003b; Jonckheere et al., 2015).

Modelling with the inclusion of RDAAM corrected (Flowers et al., 2009) AHe data, resulted in a mismatch between predicted and observed AFT age for all modelled samples, except for BR-13. For BR-27 and BR-28, the model 'broke' (i.e. displays a gap in relative probability between the higher temperature and lower temperature sections of the t-T path) and could not find a plausible solution. In general, adding AHe data results in models predicting the AHe ages well, but pushes back the predicted AFT age in time, causing the mismatch with the observed age. When comparing the prediction to the length histogram, models including AHe data seem to push the model towards longer lengths than observed. This results in models predicting a faster cooling rate to lower temperatures than with AFT data only.

Based on the failure to predict both AFT and AHe ages in Set 2, we only continued with Set 1 for joint (i.e. sample-grouped) inversion with adjacent samples (Appendix A, Fig. B.3). After a first grouping, two groups were expanded for joint inversion to cover a larger area, namely the coastal samples and the central CFZ samples. Following these modelled expected t-T paths all (grouped) samples cool from just below or just inside the lower APAZ. Most t-T paths predict a major strong phase of accelerated cooling (3–4 °C/Ma) during the Late Cretaceous to earliest Paleogene (100–60 Ma) of ~70–80 °C (Appendix A, Fig. B.3). According to the models, there is minor reheating to ~50 °C (20–5 Ma), followed by extremely rapid cooling to current temperature conditions. Samples from the Colatina Fracture Zone (Fig. 3) show a different thermal history, in which a rapid cooling between 100 Ma and 85 Ma is interrupted by a phase of slower cooling until 70–80 Ma, followed by protracted cooling. When combining BR-22, BR-23–24 and BR-25–26, the model even predicts a short reheat to the top of the partial annealing zone between 80 Ma and 65 Ma. It is unclear to which extent this is a modelling artefact. The fact that a slower cooling to minor reheat is detected in multiple samples from a same area suggests that cooling could at least have slowed down in this area during this period. Except for BR-23–24 this is again followed by a minor reheat between 40 Ma and 10 Ma and rapid (post-)Neogene cooling (Appendix A, Fig. B.3). The predicted Neogene cooling is most likely a modelling artefact, because we find no indication in the AFT data, and the sample should be 'insensitive' to this smaller magnitude of cooling when above the APAZ.

5. Discussion

5.1. Timing and depth of exhumation inferred from thermochronology

Although the Brazilian passive margin has been the subject of many studies using thermochronology, only the study area of Jelinek et al. (2014) overlaps to some extent with the one investigated here. Some of the samples from both these studies were from close proximity to each other (Fig. 4). Comparison of these samples shows that ages of the two studies lie within standard error, which allows us to expand our dataset with the AFT data from Jelinek et al. (2014).

The combined dataset shows that AFT central ages are mainly Cretaceous to early Paleogene (Fig. 4). Early Cretaceous ages are identified by Jelinek et al. (2014) in adjacent areas that were not sampled for this study (Fig. 4). High track length values and HeFTy (Ketcham, 2005) models accordingly indicate rapid denudation for these Jelinek et al. (2014) samples. The authors link this to the erosion of an uplifted rift shoulder, as it coincides with the syn-rift phase. The majority of the samples from aforementioned study in the overlapping area however fall within the Late Cretaceous–early Paleogene interval as is the case in our work. From our data, rapid basement cooling is indicated by the overall long mean confined track lengths with narrow standard deviation (Fig. 6; Appendix A, Table B.2). The minor negative skewing can be indicative of longer residence in the lower part of the partial annealing zone, or a short time of reheating in the uppermost APAZ, as existing tracks will shorten while new tracks at full length can still form within this zone. Indeed, inversion of our samples confirms a rapid cooling since the Late Cretaceous–Paleocene from the lower partial annealing zone (Fig. 9). We interpret this cooling as accelerated denudation of the basement. Thermal relaxation is excluded as a cause of cooling, since the ages are from the drift phase and thermal effects of rifting decrease rapidly with distance from the rift axis (Gallagher et al., 1994; Cogné et al., 2011). This timing of denudation was also recognised in the area previously (Jelinek et al., 2014) and in other study areas along the Brazilian passive margin (Turner et al., 2008; Cogné et al., 2011, 2012; Japsen et al., 2012a). The large-scale denudation is also supported by a sequence of Upper Cretaceous sediments of maximum 2500 m thick in the Espirito Santo Basin (Fig. 1d) (França et al., 2007).

Most of the expected t-T paths from inverse modelling (Fig. 9; Appendix A, Fig. B.3) reveal the same trend of rapid cooling between the Late Cretaceous and the Paleocene (100–60 Ma). Only samples from within the Colatina Fracture Zone and sample BR-03 show more protracted cooling since 120–100 Ma, and/or show a phase of stability within the APAZ between 100 Ma and 70 Ma (Appendix A, Fig. B.3). One possible explanation can be found in what we describe as the *prior effect* (Appendix A). In QTQt, the size of the prior will influence the outcome, resulting in more 'easy' models (protracted cooling) for larger priors. The relation of this effect to AFT age and the number of iterations should still deserve further investigation. Nonetheless, even if there is an influence of the prior effect for these samples, it should be no coincidence that samples from within the CFZ, from multiple elevations but from the same area, show this more complex t-T path. This t-T path with slowed cooling also remains when joint modelling of multiple samples of the same area is performed (Appendix A, Fig. B.3). When combining five samples (BR-22–26) from within the CFZ in one

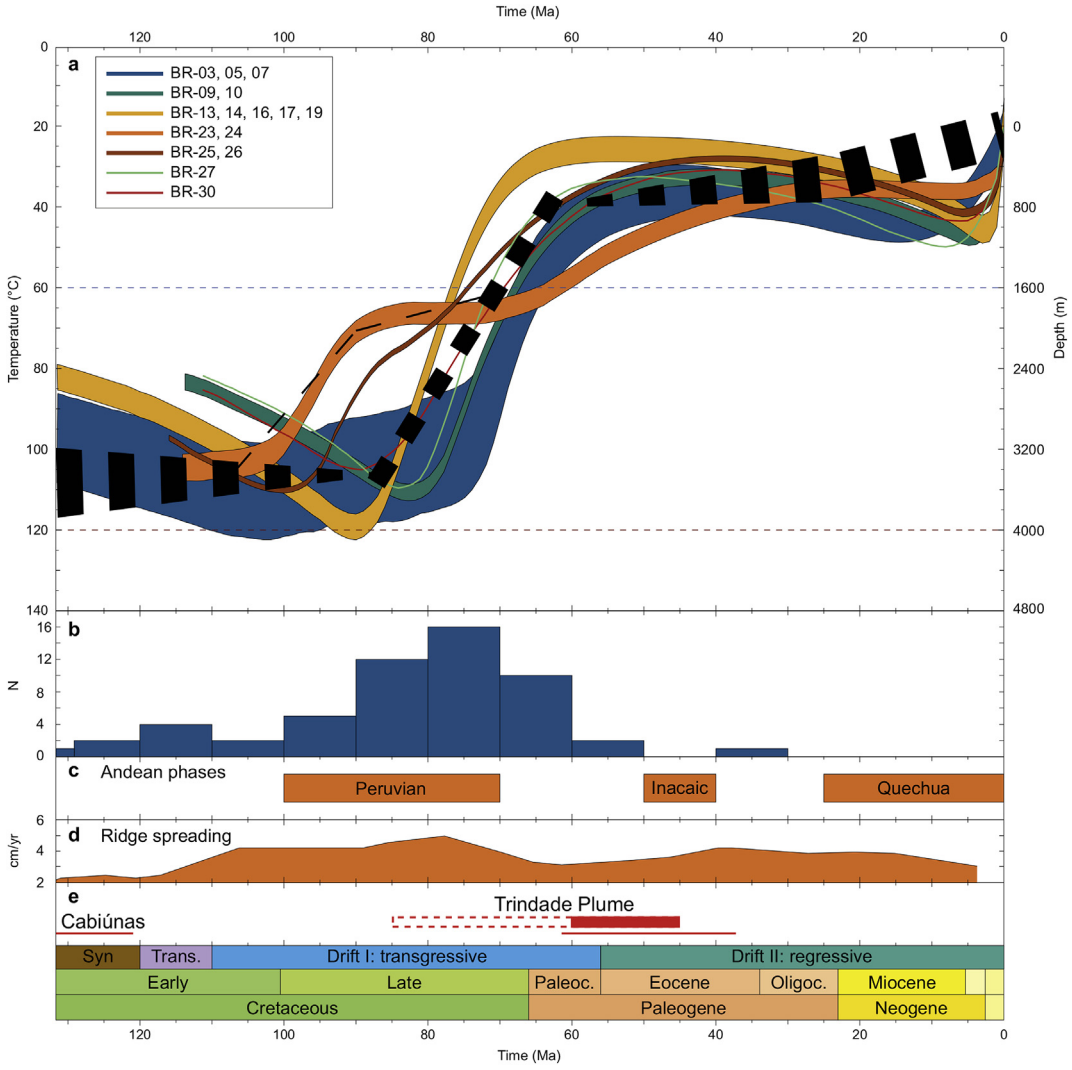

Fig. 9. Summary figure from thermochronology (full thermal history data in Appendix A) and interpretation. (a) Expected t-T paths from this study. The depth is calculated assuming a constant geothermal gradient of 25 °C/km (Hamza et al., 2005). The estimated pattern for the total area is indicated with the thick, dashed line. (b) Age-frequency distribution of this study, including ages from Jelinek et al. (2014). (c) Andean phases, from Cobbold et al. (2001). (d) Medium ridge spreading rate (Clark, 2018). (e) Offshore magmatic episodes (Line) and position of the Vitória Trindade mantle plume (Thompson et al., 1998) under the São Francisco craton (dashed box) and under the Araçuaí belt (filled box). Phases in the offshore basins are from França et al. (2007).

modelling run, this even results in a short reheat around 70 Ma. Since the length-frequency distributions (Fig. 6) do not show clear evidence of such an event and cooling ages are still similar to the ones inferred from other samples, we disregard the model with reheating. We conclude that the CFZ samples have resided longer in the upper part of the APAZ, compared to the other samples, showing simple accelerated cooling. We will further elaborate on this spatial difference in Section 5.3. Even though the different paths described by a subset of samples, the magnitude of cooling is of the same extent (Fig. 9). The expected t-T paths generally show cooling from the lower APAZ ~120–110 °C to ~60–40 °C. A generalised t-T expected model describes a cooling rate of approximately 3 °C/Ma. Following Hamza et al. (2005), the geothermal gradient on the Brazilian continental margin currently varies of 30–20 °C/km, resulting in an average of (25 ± 5)°C/km. In order to calculate an approximation of the thickness of the eroded section of basement, we adopt the simplified assumption that the geothermal gradient did not change significantly after break-up (Japsen et al., 2012a; Jelinek et al., 2014). Within this assumption, the cooling corresponds to a removal of 2.6 km of basement during the Late Cretaceous to Paleocene (Fig. 9). This corresponds to the estimate made by Japsen et al. (2012a) from north of our study area, who argue that the area was covered under a 2–3 km thick rock overburden prior to the Campanian. Jelinek et al. (2014) also report denudation of up to 2.9 km for the Mantiqueira Range. Considering the uncertainty of the models, it is also possible that samples have cooled from the bottom of the APAZ to somewhere between ~60 °C and surface temperatures (Fig. 9). A group of samples of Jelinek et al. (2014) from the Mantiqueira Range are predicted to have remained in the upper part of the APAZ. This also holds true for our samples from the CFZ where a longer residence within the top of the APAZ is predicted by the models. This leads us to the assumption that samples did not cool to temperatures far lower than the top of the APAZ during the Late Cretaceous–Paleocene, which would result in a remaining section of 2–3 km of overburden. Later removal of this overburden falls out of the AFT detection limit, but must be post early Eocene.

The assumption of a constant geothermal gradient of 25 °C/km neglects the possible thermal influence of the Trindade thermal anomaly (~85–55 Ma) (Thompson et al., 1998). This means that we

should assume an increasing geothermal gradient during denudation (Fig. 9). To the best of our knowledge, there is however no data on the adaptation of the geothermal gradient to the Trindade thermal anomaly. As such, it is not possible to provide a more correct estimation of the exhumation depth. This means that the estimated values should be regarded as a maximum for the amount of denudation.

Our expected t-T paths also predict thermal stability since the Eocene to middle Miocene, or even a minor reheating, which is followed by rapid exhumation. This is a well-known artefact of the annealing models (e.g. Jonckheere, 2003b). Furthermore, as the predicted t-T paths are already above the APAZ, samples would be insensitive to detect further denudation-induced basement cooling at that time. We thus conclude that this late Miocene–recent accelerated cooling displayed by the expected t-T paths is indeed the result of an artefact and is not unambiguously contained within our AFT data.

5.2. AFT vs. AHe

The AHe ages show the same age interval as the AFT ages, spanning the Cretaceous to early Paleogene. Besides the typical high dispersion for AHe data, for multiple samples the AHe ages are also older than the AFT age of the same sample (Fig. 8). Green and Duddy (2018) state that a good understanding and calibration of fission track annealing kinematics exists, while the diffusion kinematics of the AHe system are less clear. This would suggest that the discrepancy between these two systems is most likely explained by problems in the AHe system. AHe ages older than the AFT age are furthermore most probably indicative of an AHe closure temperature above 100 °C (Green and Duddy, 2018). Causes of this are most likely found in enhanced He retentivity. This suggests a higher closure temperature, in fact close to the AFT closure temperature, and would imply that the AHe ages do not contain additional information, but instead are equivalent to the data recorded by AFT ages. Higher dispersion and a potential lesser degree of understanding of the kinematics of this system, makes us more careful in the manner the AHe data can be interpreted here. In this regard, in general, AHe ages confirm the estimated time of exhumation as indicated by the AFT data. Due to the uncertainty on the AHe closure temperature, we are reluctant to interpret the proximity of the AHe ages to the AFT ages as rapid exhumation, as is sometimes done in literature (e.g. Ribeiro, 2007).

5.3. Spatial distribution of the ages

The spatial distribution of the AFT ages in our study area is complex, with the majority of the samples being of Late Cretaceous–Paleocene age surrounding the Late Jurassic to Early Cretaceous samples of Jelinek et al. (2014). The complex nature of the thermal history of this area is reflected and is very clear in the spatial distribution (Fig. 4). More precisely, the distance-to-coast and the age-elevation plots (Fig. 5) give a clear indication of spatially differential cooling. Most remarkable are the Late Jurassic and Early Cretaceous ages of Jelinek et al. (2014), counter-intuitively from the lowest location in the study area. The differential AFT age distribution observed here is inherently a signal of differential denudation. In general, the ages indicate that on a large scale the entire area experienced Late Cretaceous–Paleocene denudation. This is confirmed by the similar long track length distribution observed in the samples (Fig. 6). Regarding the error and the variance between samples, it is however beyond the resolution of our method to define clear groups for a smaller scale order of exhumation. Even more so for the t-T paths (Fig. 9; Appendix A, Fig. B.3), it is not possible to identify spatial groups that were exhumed earlier as compared to others.

When including the data from Jelinek et al. (2014) with our results, it is possible to roughly define three groups on the age-elevation plot (Fig. 5a). A first group is found in the higher-elevation samples from the Mantiqueira Range (Fig. 3). The second group is from the northern, lower-elevation section, including the inselberg area. These two groups appear to coincide at the Early Cretaceous ages from the northernmost Mantiqueira Range (Fig. 5a) (Jelinek et al., 2014). The samples of Jelinek et al. (2014) from along the Doce River plot in a separate group with high age and low elevation.

It was already recognised by Gunnell and Harbor (2010) that lithology, inherited geological structures and drainage have an important influence on denudation. The spatial variance of the samples could thus be explained by differential motion between fault-bounded blocks. Previous studies have already indicated the importance of reactivation of basement structures as a cause of spatial variation in thermochronology data (De Grave et al., 2007; Hiruma et al., 2010; Cogné et al., 2011, 2012; Karl et al., 2013; Glorie and De Grave, 2016). Indeed, this region contains inherited NNE–SSW trending faults and shear zones from its Neoproterozoic history (Fig. 2). It is thus likely that blocks, defined by those structural systems, were reactivated during the Late Cretaceous. N–S tilting of these blocks could furthermore induce variation within one fault-bounded block. Indeed, differential reactivation and tilting of these blocks could partly explain a pattern of ages varying in directions both parallel and perpendicular to the coast line (Fig. 4).

The reactivation of fault-bounded blocks can however not explain all of the observed variation (Figs. 4 and 5). Especially the low elevation position (Fig. 3) of the older, Late Jurassic–Early Cretaceous ages within the Doce River valley is problematic, as there is no evidence of fault-separation and furthermore block tilting would create an incompatibility with the ages of other samples (Fig. 4). As well as the Aptian samples from the northernmost part of the eastern plateau of the Mantiqueira Range (Fig. 3) within one fault-block are incompatible with Maastrichtian–Danian samples ~30 km to the south. Marent et al. (2018) found that coastal basin rivers, such as the Doce River, have high denudational capacity, and can thus be responsible for deep localised denudation. Although we have no data regarding the paleo-position of the Doce river, it can be assumed that it has not shifted greatly through time, or that a paleo-Doce river was present, analogous to other South American rivers, which are argued to have been around their present location since the Early Cretaceous (Cox, 1989; Potter, 1997). The results of differential denudation due to the location of a drainage network can be illustrated by the present geomorphology (Fig. 3), with a low-level Doce River basin surrounded by high-level plateaus. The morphology of the drainage network in itself is also partly dependent on the regional structural fabric, creating locally low elevations and weak zones that are preferentially occupied by the drainage network.

We conclude that the spatial difference between denudation times of the samples can be the result of a complex interplay between the regional structural trend and the regional drainage.

5.4. Driving forces

After break-up, cooling and thermal relaxation, one of the sources of stress on a passive margin is generated by the total offshore load, which is a result of both ageing of the oceanic crust and sediment load (Braun et al., 2013; Rouby et al., 2013). Thermal subsidence at the Brazilian margin was initiated during the Aptian in the offshore basins, and continued during the oceanic phase until

recent times (Fetter, 2009). Subsidence related to ageing of the oceanic crust, in combination with sedimentary subsidence, accommodated the deposition of up to 10 km of marine sediments in the offshore basins (Milani, 2007; Fetter, 2009). This load from both heavier, cooling oceanic lithosphere and sedimentation leads to flexural bending of the passive margin, as indeed has been proposed to explain the stress regime of the east Brazilian passive margin (Reis et al., 2013). The loading of the offshore basins and coupled flexural isostasy have a major effect on the landscape evolution of a passive margin (e.g. Kooi and Beaumont, 1994; Van der Beek et al., 1995; Burov and Cloetingh, 1997; Gilchrist and Summerfield, 1990). Computer simulations of thermal and flexural evolution of lithosphere however suggest that other processes are required to explain an increase in detrital sediment accumulation in the basins. These changes can correspond to a change in climate, erodability of the area, drainage reorganisation, or forced (tectonic) uplift (that is not the product of flexural isostasy) (Rouby et al., 2013). In our case, forced tectonic uplift and/or consequent drainage reorganisation is most likely. We also exclude climate change as a primary cause for accelerated erosional denudation, as indications on climate show that stable climate conditions prevailed throughout that period (Cogné et al., 2011; and references therein). During the Late Cretaceous–Paleocene denudation episode, the south-eastern Brazilian highlands and margin were under a NE–SW oriented strike-slip stress system (Riccomini, 1989; Ferrari, 2001; Fernandes and Amaral, 2002; Salomon et al., 2015). It must be noted that to explain this strike-slip regime, a second force is necessary, since this cannot be produced by flexural bending alone (Salomon et al., 2015). We argue that flexural bending is thus not the only major cause of the Late Cretaceous–Paleocene uplift observed in this study. On the other hand, the coupling of basins and margin through flexural bending may attribute as a positive feedback to uplift and exhumation.

A potential second force to take into account is ridge-push, exerted by the South Atlantic (Assumpçao, 1992; Harman et al., 1998; Japsen et al., 2012a). However, the Late Cretaceous exhumation phase that is recognised along the Brazilian margin, including this study area, coincides with a constant spreading rate (~6 cm/yr) to a decreasing spreading rate (Fig. 9) (Torsvik et al., 2009; Clark, 2018). This would normally result in a decrease in ridge push and not vice versa, as was already argued by Japsen et al. (2012a) for northeast Brazil. Although we do not consider stresses from the South Atlantic as a main source of the stress field in our study area, we do not disregard its influence in the total integrated sum of stresses exerted on the passive margin.

Another major force exerted on the South American plate since the Early Jurassic and still ongoing today is related to the convergent margin at the western boundary of the plate. Cobbold et al. (2007) suggested a combined effect of the South Atlantic and the East Pacific ridge push leading to the compressional regime. Far-field stresses related to the Andean orogeny have been proposed on multiple occasions to explain compressional events on the east Brazilian passive margin (e.g. Cobbold et al., 2001; Cogné et al., 2011, 2012; Karl et al., 2013). This is mainly underpinned by the coincidence of uplift events on the passive margin with major Andean tectono-orogenic phases. It is however argued that the pre-Miocene compression was less significant, since the main uplift of the Andes only started in the early Miocene (Maloney et al., 2013; Salomon et al., 2015). Indeed, effects of the flat-slab subduction are primarily well indicated after the Miocene (Jordan et al., 1983; Ramos et al., 2002). Nonetheless, the main phase of denudation of the Brazilian margin recognised in this study, coincides mostly with the Peruvian phase of the Andean orogeny (Fig. 9). To explain the lag time between the end of the Peruvian phase and t-T path stabilisation (Fig. 9) we emphasize that the AFT data register the cooling related to denudation as a response to uplift, rather than the uplift itself. Although we have no further arguments than the coincidence of denudation with the Peruvian phase, this source of stress and its timing cannot be neglected.

In paleostress studies it is also argued that stresses may be related to mantle drag, resulting from the westward shallow mantle flow originating from the South African superplume (Lima et al., 1997; Colli et al., 2013; Salomon et al., 2015; Hu et al., 2017). It is however difficult to estimate the influence of this deep system to upper crustal processes. Green et al. (2018) indicated that edge-drive convection is not likely to cause reactivation that leads to elevated margins. Recent studies have, on the other hand, demonstrated that dynamic mantle processes can have an important influence on the evolution of the lithospheric plates, through the manifestation of dynamic topography (Flament et al., 2013). In this view, the South African Platform has been attributed to positive dynamic topography related to the South African superswell (e.g. Braun et al., 2014; Brown et al., 2014; Guillocheau et al., 2018). Within the 'plume hypothesis' of Thompson et al. (1998), our study area is located over the path of the Trindade plume, which presumably passed under the region between 60 Ma and 55 Ma (Fig. 9). Analogous to the South African superswell, dynamic topography of the Trindade plume may have caused the uplift and consequential denudation during the Late Cretaceous–Paleocene. It must however be noted that cooling already starts around 90 Ma and thus before the centre of the plume head passed under the Araçuaí orogen area (Eocene, 60–55 Ma; Fig. 9). If we consider the criticism on the plume hypothesis (e.g. Ernesto et al., 2002), the uncertainty on the existence of the Trindade plume is also reflected. Consequently the ability of the Trindade plume to cause dynamic topography of the observed magnitude lies within the same uncertainty. In a more generalised context, the Trindade thermal anomaly may have contributed to the thermal weakening of the lower crust, and thus making it more susceptible to react to stress fields (Cloetingh et al., 2008; Burov and Cloetingh, 2009). Basement reactivation through far-field stresses on a thermally weakened crust was already proposed by Cobbold et al. (2001). Furthermore, the Trindade thermal anomaly is considered to be responsible for development of the volcanic Abrolhos Plateau offshore our study area (Fig. 1d). It can be expected that an offshore loading of this extent might cause a local flexural response. It must however be noted that, to put forward the effect of thermal weakening, similar regional processes are necessary to explain the large, margin-wide extent of the Late Cretaceous–Paleocene denudation event.

Considering the constraints postulated here, the south-eastern Brazilian highlands were probably prone to flexural isostasy due to the combined load of the oceanic lithosphere and the sedimentary basins. Between ~85 Ma and 55 Ma the Trindade thermal anomaly could have weakened the crustal structure further. Around the Late Cretaceous, the area was compressed through a complex interaction of ridge-push from the South Atlantic spreading, and from the Peruvian phase of the Andean orogeny. A combination of these forces interacting on the margin's lithosphere, with a lower elastic thickness (Pérez-Gussinyé et al., 2007) could have resulted in uplift of the area through reactivation of the inherited Neoproterozoic structural framework of the Araçuaí orogenic edifice. At this moment it remains unclear whether and to which extent each individual factor had a role in causing the observed uplift. We further suggest that multi-scale numerical models could be applied to provide more insight into the independent role of the here discussed forces.

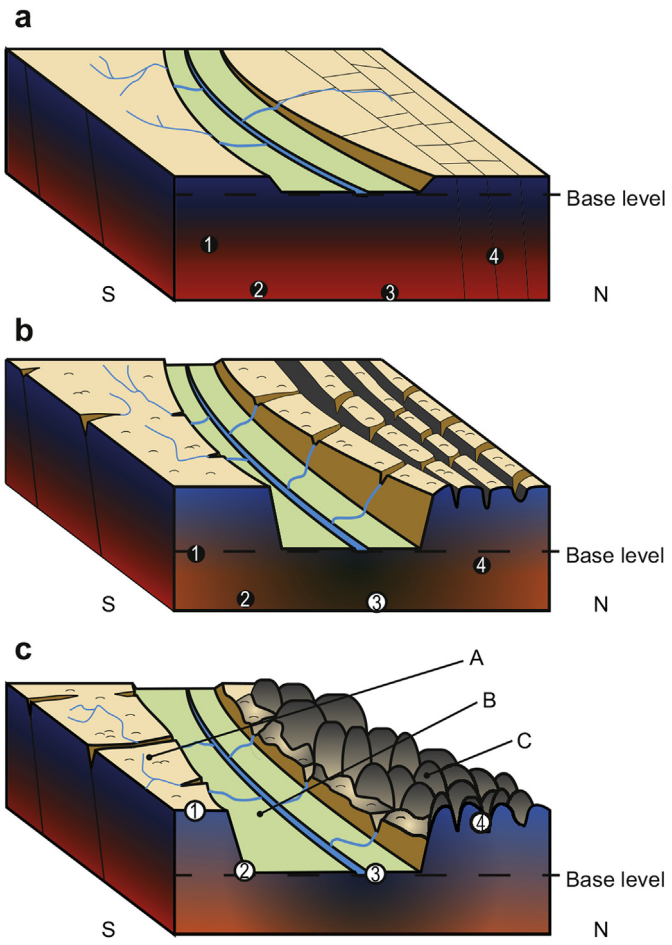

Fig. 10. Simplified conceptual model to demonstrate the effects of a two-stage differential denudation based on AFT ages. The concept of a fracture zone was added on the right side of this block diagram, analogous to the Colatina Fracture Zone. For illustrative purpose, the fracture zone in this block diagram was drawn parallel to the main river, which is a coastal basin river. Hypothetical samples are indicated with circles, numbers 1 to 4: black: below APAZ, white: above APAZ. (a) Peneplain. All samples are below the APAZ. Weathering takes place at weak zones, such as along the fractures. (b) Situation after first phase of uplift. The persistent river incises as response to the lowered base level, followed by a broadening of the river valley. Consequentially the isotherms adapt to the new topography, bulging down below the river valley. In this example, this causes sample 3 to cool below 60 °C and record the time of this first denudation phase in its AFT age. All other samples remain at elevated temperatures (>120 °C). Weathered material is removed from the fractures. (c) Situation after second phase of uplift and further maturation of the landscape. After uplift, the river again incises rapidly. Denudation causes all samples to cool below APAZ temperatures. Further maturation (erosion and transport) of the landscape causes the river valley to expand (B; scarp retreat of elevated plateau). Through continuing denudation, samples become exhumed. Protracted uplift may contribute to the persistence of the elevated plateau (A). Preferential removal of material along fractures and exfoliation lead to the emergence of inselbergs (C).

5.5. Formation of the current landscape

Although Braun (2018) already showed that reconstructing landscape evolution solely on the basis of low-temperature thermochronology (and exposure dating) is hazardous, it can however set some constraints. Here we will draft a hypothesis on the landscape evolution of the area defined by the Araçuaí orogen lithotectonic units since break-up and as constrained by our data.

During the Early Cretaceous, the Araçuaí orogen area evolved to an active continental rift setting, with the development of rift shoulders. The oldest AFT ages suggest that part of this rift shoulder was eroded away locally, probably due to the erosive power of a paleo-Doce river and its tributaries. Fig. 10 illustrates this process in a generalised block model. Since the conditions leading to this large erosive power could have been initiated since the formation of a rift basin, we can assume that a river of this magnitude can indeed cause localised denudation. We assume that the primary drainage pattern has since remained approximately at this position, as analogous to most South American river systems (Cox, 1989; Potter, 1997). The course of the drainage was most likely determined at least partly by the pre-existing structural framework, such as is the case today (Cohen et al., 2014).

Considering AFT and AHe ages and long track lengths of the Late Cretaceous–Paleocene samples described earlier, they must have remained below or in the lowermost section of the APAZ during the Early Cretaceous (Fig. 10). During the Late Cretaceous–Paleocene, the area most likely reacted to compressional events as those described in the previous section, with uplift and reactivation of the fault system. Our models predict that a rock overburden of 2–3 km of basement has been eroded and must have been transported as detrital material to the offshore basins during this uplift and denudation event (Fig. 9). Analogous to the Early Cretaceous, we can assume that the Doce River incised quickly as a response to the change in base level. Rapid incision of the Doce River is also supported by samples BR-19 and BR-22, which are from lower elevation, but also exhibit Late Cretaceous ages, same as from the higher elevated areas. Within this scenario, the Early Cretaceous ages constrain the maximum uplift of the Late Cretaceous–Paleocene to ~2 km, as they would otherwise have resided within the top of the APAZ, which contradicts their track length distribution. This model for denudation would then allow for a remaining overburden of maximum ~2 km thickness on the Mantiqueira Range and the inselberg area. Since our samples are at the surface today, this section must have been removed between the early Eocene and recent times.

Evidence of ongoing denudation after the Paleocene is found in the sedimentary log of the Espirito Santo Basin (Fig. 1d), reaching a maximum thickness of 2500 m since the late Eocene, or even 4100 m since the Cretaceous–Paleocene transition (França et al., 2007). This thick sequence of sediments is not necessarily the result of increased denudation in our study area, but could as well partly be related to a lowering base level due to protracted flexure, eustatic sea level (Miller et al., 2005, 2011) and expansion of the catchment area of the drainage (reorganisation) towards the Espirito Santo Basin (Rouby et al., 2013). Further maturation of the landscape, such as erosion of the elevated plateaus also contributes to sediment transport to the Espirito Santo Basin. Clear tectonic reactivation has been recognised during the Quaternary (Cherem et al., 2012; Cohen et al., 2014), indicating that the passive margin may indeed have been active during at least the late Cenozoic, though we assume only to a minor extent, i.e. not visible in the AFT data.

Although the Mantiqueira Range and the northern inselberg area are different in geomorphology, they exhibit a same interval of AFT cooling ages, indicating that they were exhumed at roughly the same time. The main difference of the northern section is the presence of the Colatina Fracture Zone, which crosscuts the Neoproterozoic trend in a NW–SE direction (Fig. 3). This dense fracture network has shaped the inselberg region by weathering and thus enhanced erosion nucleating from the fractures (Owen, 2014; Chicarino Varajão and Alkmim, 2015), of which the result is illustrated in Fig. 10. Erosion along this dense fracture network and denudation by the incision of the Doce River and tributaries can indeed explain the formation of the low-relief and inselberg areas. An explanation however lacks for the longevity of the Mantiqueira Range (Fig. 3), as there are no lithological grounds to attribute its enhanced resistance to erosion (Fig. 2). Through modelling of

passive margin escarpment evolution, it was found that flexural isostasy plays a major role in controlling whether an escarpment becomes a drainage divide, such as the Mantiqueira Range. This has a large influence on the stability of the escarpment (Braun, 2018). We further argue that the Mantiqueira Range was shielded from erosion by the differential reactivation of the Neoproterozoic NNE–SSW structural trend, which also forms the Doce River graben (Mello et al., 1999; Cherem et al., 2012). Just south of Governador Valadáres the Doce River markedly changes direction towards the southeast (Fig. 3), following the Cambrian ESE–WNW lineaments, that likely reactivated during the Early Cretaceous and may have captured the Doce River, directing transport towards the Espirito Santo Basin. At the weak zone of the CFZ, the Doce River changes course in E–W direction. Sample BR-30 (Fig. 3) illustrates that the Doce River must have undergone changes of secondary magnitude of its path during the latest Late Cretaceous (Fig. 4).

6. Conclusions

We presented new apatite fission track (AFT) and apatite U–Th/He (AHe) data from the south-eastern Brazilian highlands underlain by the Araçuaí orogen lithotectonic units, i.e. the central east Brazilian passive margin onshore sector. Both AFT and AHe central ages are Late Cretaceous to early Paleogene. Fission track lengths are generally long (~ 13 μm), showing a unimodal distribution with minor negative skewness, indicative of fast basement cooling. Based on our data, we conclude that:

(1) AHe ages are highly dispersed, with in general an absence of age-eU and age-R^* correlations, and AHe ages scatter around AFT ages, probably caused by limited U(/Th)-zoning, crystal defects and/or U/Th-rich micro-inclusions. This causes AFT-AHe joint inversion to fail. We argue that due to enhanced He retention AHe ages are equivalent to AFT closure temperatures and hence to AFT ages, rather than complementary, although the former exhibit a much larger source of uncertainty.
(2) The south-eastern Brazilian highlands have experienced a major phase of uplift and accelerated denudation during the Late Cretaceous to early Paleogene, through a reactivation of the regional structural framework. Estimates based on inversion indicate a removal of 2–3 km of overburden. This event probably pre-shaped the current landscape.
(3) We emphasize the uncertainty of cooling events after the Paleocene. Based on the landscape characterised by the inselbergs, the removed section of the Doce River basin and the Cenozoic deposits in the Espirto Santo Basin, we argue that (limited) Cenozoic uplift has taken place.
(4) We explain spatial variance in AFT ages through spatially differential denudation, partly linked to differential reactivation of the basement structural framework of the Araçuaí orogen and impact from the drainage network. This framework also has a major influence on the small-scale denudation, which has led to the formation of the inselberg landscape of the inselberg area, the Doce River Basin and the persisted role of the Mantiqueira Range as a drainage divide.
(5) By reviewing the range of forces that have been and are working on the region, we find indications that most probably the margin reactivated under a compressive regime during the Late Cretaceous, both from the Peruvian phase of the Andean orogeny and high spreading velocity of the Mid-Atlantic Ridge. Probably the crust was also weakened by the Trindade thermal anomaly, making it more susceptible to the compressional deformation. The combination may have caused a reactivation of the basement structures, although it is uncertain whether and to which degree each of the discussed forces is responsible.
(6) We suggest that, to understand the thermo-tectonic history of the Araçuaí orogen region, multi-scale numerical modelling can be a great asset to test hypotheses with different parameters, constrained by data from thermochronology.

Acknowledgements

This work was supported by the Special Research Fund of Ghent University (BOF 01N03915). Many thanks to Dr. Eugenia Toimil Molares and the GSI Helmholtz Centre for Heavy Ion Research for the LINAC heavy iron irradiation of the samples. We thank Bart Van Houdt of SCK·CEN for the help with the thermal neutron irradiation of the samples. James Schwanetahl from University College London is acknowledged for the improvement and maintenance of the He measurement equipment and his explanations and help on it. We thank Andy Carter of Birbeck University for providing U–Th measurements for AHe. Our gratitude goes out to Ann-Eline Debeer, our lab technician, who carefully separated the samples for this study. A.C. Pedrosa-Soares and T. Novo thank the Brazilian Research Council (CNPq) for their productivity grants. We also wish to thank the three anonymous reviewers whose comments helped to improve this paper.

Appendix A. Supplementary data

Supplementary data to this article can be found online at https://doi.org/10.1016/j.gsf.2019.05.011.

References

Aguilar, C., Alkmim, F.F., Lana, C., Farina, F., 2017. Palaeoproterozoic assembly of the São Francisco craton, SE Brazil: new insights from U–Pb titanite and monazite dating. Precambrian Res. 289, 95–115. https://doi.org/10.1016/j.precamres.2016.12.001.

Alkmim, F.F., Marshak, S., Pedrosa-Soares, A.C., Peres, G.G., Cruz, S.C.P., Whittington, A., 2006. Kinematic evolution of the araçuaí-west Congo orogen in Brazil and Africa: nutcracker tectonics during the neoproterozoic assembly of Gondwana. Precambrian Res. 149, 43–64. https://doi.org/10.1016/j.precamres.2006.06.007.

Alkmim, F.F., Teixeira, W., 2017. The paleoproterozoic mineiro belt and the quadrilátero ferrífero. In: São Francisco Craton, Eastern Brazil. Regional Geology Reviews. Springer, Cham, pp. 71–94. https://doi.org/10.1007/978-3-319-01715-0_5.

Almeida, F.F.M., 1977. O cráton do São Francisco. Rev. Bras. Geociencias 7, 349–364.

Almeida, F.F.M., 1991. O alinhamento magmatico de Cabo Frio. In: 2°. Simposio de Geologia Do Sudeste. São Paulo, Brazil, pp. 423–428 (in Portuguese).

Alves, T.M., Cartwright, J., Davies, R.J., 2009. Faulting of salt-withdrawal basins during early halokinesis: effects on the paleogene Rio Doce canyon system (espírito Santo basin, Brazil). Am. Assoc. Petrol. Geol. Bull. 93, 617–652. https://doi.org/10.1306/02030908105.

Asmus, H.E., Gomes, J.B., Pereira, A.C.B., 1971. Integração geológica regional da bacia do Espíroto Santo. In: Anais Do XXV Congresso Brasileiro de Geologia (SBG). São Paulo, Brazil, pp. 235–254 (in Portuguese).

Assumpçao, M., 1992. The regional intraplate stress field in South America. J. Geophys. Res. 97, 11889. https://doi.org/10.1029/91JB01590.

Barbarand, J., Carter, A., Wood, I., Hurford, T., 2003a. Compositional and structural control of fission-track annealing in apatite. Chem. Geol. 198, 107–137. https://doi.org/10.1016/S0009-2541(02)00424-2.

Barbarand, J., Hurford, T., Carter, A., 2003b. Variation in apatite fission-track length measurement: implications for thermal history modelling. Chem. Geol. 198, 77–106. https://doi.org/10.1016/S0009-2541(02)00423-0.

Belém, J., 2014. Geoquímica, Geocronologia e contexto geotectônico do magmatismo máfico associado ao feixe de fraturas Colatina, Estado do Espírito Santo. PhD Thesis. Universidade Federal de Minas Gerais, p. 138 (in Portuguese).

Belton, D.X., Brown, R.W., Kohn, B.P., Fink, D., Farley, K.A., 2004. Quantitative resolution of the debate over antiquity of the central Australian landscape: implications for the tectonic and geomorphic stability of cratonic interiors. Earth Planet. Sci. Lett. 219, 21–34. https://doi.org/10.1016/S0012-821X(03)00705-2.

Bertotti, A.L., Chemale, F., Sylvester, P.J., Kayser, V.T., Gruber, L., 2014. Changing provenance of late Jurassic to early Cretaceous rift-related sedimentary rocks of The south atlantic margin: LA-MC-ICPMS U-Pb and Lu-Hf isotopic study of detrital zircons from the Camamu basin, eastern Brazil. Chem. Geol. 363, 250–261. https://doi.org/10.1016/j.chemgeo.2013.10.030.

Braun, J., 2018. A review of numerical modeling studies of passive margin escarpments leading to a new analytical expression for the rate of escarpment

migration velocity. Gondwana Res. 53, 209–224. https://doi.org/10.1016/j.gr.2017.04.012.
Braun, J., Deschamps, F., Rouby, D., Dauteuil, O., 2013. Flexure of the lithosphere and the geodynamical evolution of non-cylindrical rifted passive margins: results from a numerical model incorporating variable elastic thickness, surface processes and 3D thermal subsidence. Tectonophysics 604, 72–82. https://doi.org/10.1016/j.tecto.2012.09.033.
Braun, J., Guillocheau, F., Robin, C., Baby, G., Jelsma, H., 2014. Rapid erosion of the South African Plateau as it climbs over a mantle superswell. J. Geophys. Res. Solid Earth 120, 1–29. https://doi.org/10.1002/2014JB010998.
Brown, R.W., Beucher, R., Roper, S., Persano, C., Stuart, F., Fitzgerald, P., 2013. Natural age dispersion arising from the analysis of broken crystals. Part I: theoretical basis and implications for the apatite (U-Th)/He thermochronometer. Geochem. Cosmochim. Acta 122, 478–497. https://doi.org/10.1016/j.gca.2013.05.041.
Brown, R.W., Summerfield, M., Gleadow, A.J.W., Gallagher, K., Carter, A., Beucher, R., Wildman, M., 2014. Intracontinental deformation in southern Africa during the late Cretaceous. J. Afr. Earth Sci. 100, 20–41. https://doi.org/10.1016/j.jafrearsci.2014.05.014.
Brown, R.W., Summerfield, M.A., Gleadow, A.J.W., 2002. Denudational history along a transect across the Drakensberg Escarpment of southern Africa derived from apatite fission track thermochronology. J. Geophys. Res. Solid Earth 107. ETG 10-1-ETG 10-18. https://doi.org/10.1029/2001JB000745.
Bruhn, C.H.L., Walker, R.G., 1997. Internal architecture and sedimentary evolution of coarse-grained, turbidite channel-levee complexes, early Eocene regência canyon, Espirito Santo basin, Brazil. Sedimentology 44, 17–46. https://doi.org/10.1111/j.1365-3091.1997.tb00422.x.
Burke, K., Sengör, A.M.C., 1988. Ten metre global sea-level change associated with South Atlantic Aptian salt deposition. Mar. Geol. 83, 309–312. https://doi.org/10.1016/0025-3227(88)90064-3.
Burov, E., Cloetingh, S., 1997. Post-rift evolution of extensional basins. Earth Planet. Sci. Lett. 150, 7–26. https://doi.org/10.1016/S0012-821X(97)00069-1.
Burov, E., Cloetingh, S., 2009. Controls of mantle plumes and lithospheric folding on modes of intraplate continental tectonics: differences and similarities. Geophys. J. Int. 178, 1691–1722. https://doi.org/10.1111/j.1365-246X.2009.04238.x.
Calegari, S.S., Neves, M.A., Guadagnin, F., França, G.S., Vincentelli, M.G.C., 2016. The Alegre Lineament and its role over the tectonic evolution of the Campos Basin and adjacent continental margin, Southeastern Brazil. J. South Am. Earth Sci. 69, 226–242. https://doi.org/10.1016/j.jsames.2016.04.005.
Carlson, W.D., Donelick, R.A., Ketcham, R.A., 1999. Variability of apatite fission-track annealing kinetics: I. Experimental results. Am. Mineral. 84, 1213–1223. https://doi.org/10.2138/am-1999-0901.
Chang, H.K., Kowsmann, R.O., Bender, A.A., Ferreira Figueiredo, A.M., 1992. Tectonics and stratigraphy of the East Brazilian Rift system: an overview. Geodaynamics Rift 213, 97–138. https://doi.org/10.1016/0040-1951(92)90253-3.
Cherem, L.F.S., Varajão, C.A.C., Braucher, R., Bourlés, D., Salgado, A.A.R., Varajão, A.C., 2012. Long-term evolution of denudational escarpments in southeastern Brazil. Geomorphology 173–174, 118–127. https://doi.org/10.1016/j.geomorph.2012.06.002.
Chicarino Varajão, C.A., Alkmim, F.F., 2015. Pancas: the kingdom of bornhardts. In: Vieira, B.C., Rodrigues Salgado, A.A., Cordeiro Santos, L.J. (Eds.), Landscapes and Landforms of Brazil. Springer, pp. 381–388. https://doi.org/10.1007/978-94-017-8023-0.
Clark, S.R., 2018. Uncertainty in the breakup, spreading history, and velocity variations of Gondwana. Gondwana Res. 53, 189–196. https://doi.org/10.1016/j.gr.2017.04.029.
Cloetingh, S., Beekman, F., Ziegler, P.A., van Wees, J.-D., Sokoutis, D., 2008. Post-rift compressional reactivation potential of passive margins and extensional basins. Geol. Soc. London, Spec. Publ. 306, 27–70. https://doi.org/10.1144/SP306.2.
Cobbold, P.R., Meisling, K.E., Mount, V.S., 2001. Reactivation of an obliquely rifted margin, Campos and Santos basins, southeastern Brazil. Am. Assoc. Petrol. Geol. Bull. 85, 1903–1924. https://doi.org/10.1306/8626D0B3-173B-11D7-8645000102C1865D.
Cobbold, P.R., Rossello, E.A., Roperch, P., Arrriagada, C., Gómez, L.A., Lima, C., 2007. Distribution, timing, and causes of Andean deformation across South America. In: Ries, A.C., Butler, R.W.H., Graham, R.H. (Eds.), Deformation of the Continental Crust. Geological Society, London, pp. 321–343. https://doi.org/10.1144/GSL.SP.2007.272.01.17.
Cogné, N., Gallagher, K., Cobbold, P.R., 2011. Post-rift reactivation of the onshore margin of southeast Brazil: evidence from apatite (U-Th)/He and fission-track data. Earth Planet. Sci. Lett. 309, 118–130. https://doi.org/10.1016/j.epsl.2011.06.025.
Cogné, N., Gallagher, K., Cobbold, P.R., Riccomini, C., Gautheron, C., 2012. Post-breakup tectonics in southeast Brazil from thermochronological data and combined inverse-forward thermal history modeling. J. Geophys. Res. 117, 1–16. https://doi.org/10.1029/2012JB009340.
Cohen, M.C.L., França, M.C., de Fátima Rossetti, D., Pessenda, L.C.R., Giannini, P.C.F., Lorente, F.L., Junior, A.Á.B., Castro, D., Macario, K., 2014. Landscape evolution during the late quaternary at the Doce river mouth, espírito Santo state, southeastern Brazil. Palaeogeogr. Palaeoclimatol. Palaeoecol. 415, 48–58. https://doi.org/10.1016/j.palaeo.2013.12.001.
Colli, L., Fichtner, A., Bunge, H., 2013. Full waveform tomography of the upper mantle in the South Atlantic region: imaging a westward fluxing shallow asthenosphere? Tectonophysics 604, 26–40. https://doi.org/10.1016/j.tecto.2013.06.015.
Cordani, U.G., 1970. Idade do vulcanismo No oceano atlântico sul. Bol. do Inst. Geociências e Astron. da Univ. São Paulo 1, 9–76 (in Portuguese).
Cox, K.G., 1989. The role of mantle plumes in the development of continental drainage patterns. Nature 342, 873–877. https://doi.org/10.1038/342873a0.
Danisík, M., Sachsenhofer, R.F., Privalov, V.A., Panova, E.A., Frisch, W., Spiegel, C., 2008. Low-temperature thermal evolution of the Azov Massif (Ukrainian Shield-Ukraine) - implications for interpreting (U-Th)/He and fission track ages from cratons. Tectonophysics 456, 171–179. https://doi.org/10.1016/j.tecto.2008.04.022.
Degler, R., Pedrosa-Soares, A., Novo, T., Tedeschi, M., Carlos Silva, L., Dussin, I., Lana, C., 2018. Rhyacian-Orosirian isotopic records from the basement of the Araçuaí-Ribeira orogenic system (SE Brazil): Links in the Congo-São Francisco palaeocontinent. Precambrian Res. 317, 179–195.
De Grave, J., Buslov, M.M., Van den haute, P., 2007. Distant effects of India-Eurasia convergence and Mesozoic intracontinental deformation in Central Asia: constraints from apatite fission-track thermochronology. J. Asian Earth Sci. 29, 188–204. https://doi.org/10.1016/j.jseaes.2006.03.001.
De Grave, J., Van den haute, P., 2002. Denudation and cooling of the lake teletskoye region in the Altai mountains (south Siberia) as revealed by apatite fission-track thermochronology. Tectonophysics 349, 145–159. https://doi.org/10.1016/S0040-1951(02)00051-3.
de Wit, M.J., Jeffery, M., Bergh, H., Nicolaysen, L., 1988. Geological Map of Sectors of Gondwana, Reconstructed to Their Disposition ~150 Ma, Scale 1: 10.000.000. Am. Assoc. Pet. Geol. Tulsa, OK, USA. Univ. Witwatersrand, Johannesburg, South Africa.
Demercian, S., Szatmari, P., Cobbold, P.R., 1993. Style and pattern of salt diapirs due to thin-skinned gravitational gliding, Campos and Santos basins, offshore Brazil. Tectonophysics 228, 393–433. https://doi.org/10.1016/0040-1951(93)90351-J.
Donelick, R.A., 1993. Apatite etching characteristics versus chemical composition. Nucl. Tracks Radiat. Meas. 21, 604.
Engelmann de Oliveira, C.H., Jelinek, A.R., Chemale, F.J., Bernet, M., 2016a. Evidence of post-Gondwana breakup in Southern Brazilian Shield: insights from apatite and zircon fission track thermochronology. Tectonophysics 666, 173–187. https://doi.org/10.1016/j.tecto.2015.11.005.
Engelmann de Oliveira, C.H., Jelinek, A.R., Chemale, F.J., Cupertino, J.A., 2016b. Thermotectonic history of the southeastern Brazilian margin: evidence from apatite fission track data of the offshore Santos Basin and continental basement. Tectonophysics 685, 21–34. https://doi.org/10.1016/j.tecto.2016.07.012.
Ernesto, M., Marques, L.S., Piccirillo, E.M., Molina, E.C., Ussami, N., Comin-Chiaramonti, P., Bellieni, G., 2002. Paraná Magmatic Province-Tristan da Cunha plume system: fixed versus mobile plume, petrogenetic considerations and alternative heat sources. J. Volcanol. Geotherm. Res. 118, 15–36. https://doi.org/10.1016/S0377-0273(02)00248-2.
Farley, K.A., 2000. Helium diffusion from apatite: general behavior as illustrated by Durango fluorapatite. J. Geophys. Res. Solid Earth 105, 2903–2914. https://doi.org/10.1029/1999JB900348.
Farley, K.A., 2002. (U-Th)/He dating: techniques, calibrations, and applications. Rev. Mineral. Geochem. 47, 819–844. https://doi.org/10.2138/rmg.2002.47.18.
Farley, K.A., Shuster, D.L., Ketcham, R.A., 2011. U and Th zonation in apatite observed by laser ablation ICPMS, and implications for the (U-Th)/He system. Geochem. Cosmochim. Acta 75, 4515–4530. https://doi.org/10.1016/j.gca.2011.05.020.
Farley, K.A., Stockli, D.F., 2002. (U-Th)/He dating of phosphates: apatite, monazite, and xenotime. Reviews in Mineralogy and Geochemistry 48 (1), 559–578.
Feinstein, S., Kohn, B., Osadetz, K., Everitt, R., O'Sullivan, P., 2009. Variable phanerozoic thermal history in the southern Canadian shield: evidence from an apatite fission track profile at the underground research laboratory (URL), Manitoba. Tectonophysics 475, 190–199. https://doi.org/10.1016/j.tecto.2009.01.016.
Fernandes, A.J., Amaral, G., 2002. Cenozoic tectonic events at the border of the Paraná basin, São paulo, Brazil. J. South Am. Earth Sci. 14, 911–931.
Ferrari, A.L., 2001. Evolução Tectônica do Graben da Guanabara. University of São Paulo (in Portuguese).
Fetter, M., 2009. The role of basement tectonic reactivation on the structural evolution of Campos Basin, offshore Brazil: evidence from 3D seismic analysis and section restoration. Mar. Pet. Geol. 26, 873–886. https://doi.org/10.1016/j.marpetgeo.2008.06.005.
Fiduk, J.C., Brush, E.R., Anderson, L.E., Gibbs, P.B., Rowan, M.G., 2004. Salt deformation, magmatism, and hydrocarbon prospectivity in the Espirito Santo Basin, offshore Brazil. In: Post, P.J., et al. (Eds.), Salt-Sediment Interactions and Hydrocarbon Prospectivity: Concepts, Applications, and Case Studies for the 21st Century, pp. 370–392.
Fitzgerald, P.G., Baldwin, S.L., Webb, L.E., O'Sullivan, P.B., 2006. Interpretation of (U-Th)/He single grain ages from slowly cooled crustal terranes: a case study from the Transantarctic Mountains of southern Victoria Land. Chem. Geol. 225, 91–120. https://doi.org/10.1016/j.chemgeo.2005.09.001.
Flament, N., Gurnis, M., Muller, R.D., 2013. A review of observations and models of dynamic topography. Lithosphere 5, 189–210. https://doi.org/10.1130/L245.1.
Flowers, R.M., Bowring, S.A., Reiners, P.W., 2006. Low long-term erosion rates and extreme continental stability documented by ancient (U-Th)/He dates. Geology 34, 925–928. https://doi.org/10.1130/G22670A.1.
Flowers, R.M., Kelley, S.A., 2011. Interpreting data dispersion and " inverted" dates in apatite (U-Th)/He and fission-track datasets: an example from the US mid-continent. Geochem. Cosmochim. Acta 75, 5169–5186. https://doi.org/10.1016/j.gca.2011.06.016.

Flowers, R.M., Ketcham, R.A., Shuster, D.L., Farley, K.A., 2009. Apatite (U-Th)/He thermochronometry using a radiation damage accumulation and annealing model. Geochem. Cosmochim. Acta 73, 2347–2365. https://doi.org/10.1016/j.gca.2009.01.015.

Fonte-Boa, T.M.R., Novo, T.A., Pedrosa-Soares, A.C., Dussin, I.A., 2017. Records of Mesoproterozoic taphrogenic events in the eastern basement of the Araçuaí Orogen, southeast Brazil. Brazilian J. Geol. 47, 447–466. https://doi.org/10.1590/2317-4889201720170045.

França, R.L., Del Rey, A.C., Tagliari, C.V., Brandão, J.R., De Rossi Fontanelli, P., 2007. Bacia do espírito Santo. Bol. Geociencias Petrobras 15, 501–509 (in Portuguese).

Franco-Magalhães, A.O.B., Hackspacher, P.C., Glasmacher, U.A., Saad, A.R., 2010. Rift to post-rift evolution of a "'passive'" continental margin: the Ponta Grossa Arch, SE Brazil. Int. J. Earth Sci. 99, 1599–1613. https://doi.org/10.1007/s00531-010-0556-8.

Galbraith, R.F., 2005. Statistics for Fission Track Analysis. Chapman & Hall/CRC.

Galbraith, R.F., Laslett, G.M., 1993. Statistical models for mixed fission track ages. Nucl. Tracks Radiat. Meas. 21, 459–470. https://doi.org/10.1016/1359-0189(93)90185-C.

Gallagher, K., 2012. Transdimensional inverse thermal history modeling for quantitative thermochronology. J. Geophys. Res. 117, 1–16. https://doi.org/10.1029/2011JB008825.

Gallagher, K., Brown, R.W., 1997. The onshore record of passive margin evolution. J. Geol. Soc. London. 154, 451–457. https://doi.org/10.1144/gsjgs.154.3.0451.

Gallagher, K., Charvin, K., Nielsen, S., Sambridge, M., Stephenson, J., 2009. Markov chain Monte Carlo (MCMC) sampling methods to determine optimal models, model resolution and model choice for Earth Science problems. Mar. Pet. Geol. 26, 525–535. https://doi.org/10.1016/j.marpetgeo.2009.01.003.

Gallagher, K., Hawkesworth, C.J., Mantovani, M.S.M., 1994. The denudation history of the onshore continental-margin of SE Brazil inferred from apatite fission-track data. J. Geophys. Res. Earth 99, 18117–18145.

Gallagher, K., Hawkesworth, C.J., Mantovani, M.S.M., 1995. Denudation, fission track analysis and the long-term evolution of passive margin topography: application to the southeast Brazilian margin. J. South Am. Earth Sci. 8, 65–77. https://doi.org/10.1016/0895-9811(94)00042-Z.

Gautheron, C., Barbarand, J., Ketcham, R.A., Tassan-Got, L., van der Beek, P.A., Pagel, M., Pinna-Jamme, R., Couffignal, F., Fialin, M., 2013. Chemical influence on α-recoil damage annealing in apatite: implications for (U–Th)/He dating. Chem. Geol. 351, 257–267. https://doi.org/10.1016/j.chemgeo.2013.05.027.

Gerin, C., Gautheron, C., Oliviero, E., Bachelet, C., Mbongo Djimbi, D., Seydoux-Guillaume, A.M., Tassan-Got, L., Sarda, P., Roques, J., Garrido, F., 2017. Influence of vacancy damage on He diffusion in apatite, investigated at atomic to mineralogical scales. Geochem. Cosmochim. Acta 197, 87–103. https://doi.org/10.1016/j.gca.2016.10.018.

Gilchrist, A.R., Summerfield, M.A., 1990. Differential denudation and flexural isostasy in formation of rifted margin upwarps. Nature 346, 739–742.

Gleadow, A.J.W., Duddy, I.R., 1981. A natural long-term track annealing experiment for apatite. Nucl. Tracks 5, 169–174. https://doi.org/10.1016/0191-278X(81)90039-1.

Gleadow, A.J.W., Duddy, I.R., Green, P.F., Hegarty, K.A., 1986a. Fission track lengths in the apatite annealing zone and the interpretation of mixed ages. Earth Planet. Sci. Lett. 78, 245–254.

Gleadow, A.J.W., Duddy, I.R., Green, P.F., Lovering, J.F., 1986b. Confined fission track lengths in apatite: a diagnostic tool for thermal history analysis. Contrib. Mineral. Petrol. 94, 405–415. https://doi.org/10.1007/BF00376334.

Glorie, S., De Grave, J., 2016. Exhuming the Meso-Cenozoic Kyrgyz Tianshan and Siberian Altai-Sayan: a review based on low-temperature thermochronology. Geosci. Front. 7, 155–170. https://doi.org/10.1016/j.gsf.2015.04.003.

Glorie, S., De Grave, J., Buslov, M.M., Elburg, M.A., Stockli, D.F., Gerdes, A., Van den haute, P., 2010. Multi-method chronometric constraints on the evolution of the northern Kyrgyz Tien Shan granitoids (central asian orogenic belt): from emplacement to exhumation. J. Asian Earth Sci. 38, 131–146. https://doi.org/10.1016/j.jseaes.2009.12.009.

Glorie, S., De Grave, J., Buslov, M.M., Zhimulev, F.I., Elburg, M.A., Van den haute, P., 2012. Structural control on Meso-Cenozoic tectonic reactivation and denudation in the Siberian Altai: insights from multi-method thermochronometry. Tectonophysics 544–545, 75–92. https://doi.org/10.1016/j.tecto.2012.03.035.

Glotzbach, C., Braun, J., van der Beek, P.A., 2015. A Fourier approach for estimating and correcting the topographic perturbation of low-temperature thermochronological data. Tectonophysics 649, 115–129. https://doi.org/10.1016/j.tecto.2015.03.005.

Gradim, C., Roncato, J., Pedrosa-Soares, A.C., Cordani, U.G., Dussin, I.A., Alkmim, F.F., Queiroga, G., Jacobsohn, T., da Silva, L.C., Babinski, M., 2014. The hot back-arc zone of the Araçuaí orogen, Eastern Brazil: from sedimentation to granite generation. Brazilian J. Geol. 44, 155–180. https://doi.org/10.5327/Z2317-4889201400010012.

Green, P.F., 1981. A new look at statistics in fission-track dating. Nucl. Tracks 5, 77–86. https://doi.org/10.1016/0191-278X(81)90029-9.

Green, P.F., 1986. On the thermo-tectonic evolution of Northern England: evidence from fission track analysis. Geol. Mag. 123, 493–506. https://doi.org/10.1017/S0016756800035081.

Green, P.F., Crowhurst, P.V., Duddy, I.R., Japsen, P., Holford, S.P., 2006. Conflicting (U-Th)/He and fission track ages in apatite: enhanced He retention, not anomalous annealing behaviour. Earth Planet. Sci. Lett. 250, 407–427. https://doi.org/10.1016/j.epsl.2006.08.022.

Green, P.F., Duddy, I., 2018. Apatite (U-Th-Sm)/He thermochronology on the wrong side of the tracks. Chem. Geol. 488, 21–33. https://doi.org/10.1016/j.chemgeo.2018.04.028.

Green, P.F., Duddy, I.R., Gleadow, A.J.W., Tingate, P.R., Laslett, G.M., 1986. Thermal annealing of fission tracks in apatite. 1. A qualitative description. Chem. Geol. Isot. Geosci. Sect. 59, 237–253. https://doi.org/10.1016/0168-9622(86)90074-6.

Green, P.F., Japsen, P., Chalmers, J.A., Bonow, J.M., Duddy, I.R., 2018. Post-breakup burial and exhumation of passive continental margins: seven propositions to inform geodynamic models. Gondwana Res. 53, 58–81. https://doi.org/10.1016/j.gr.2017.03.007.

Green, P.F., Lidmar-bergström, K., Japsen, P., Bonow, J.M., Chalmers, J.A., 2013. Stratigraphic landscape analysis, thermochronology and the episodic development of elevated passive continental margins. Geol. Surv. Den. Greenl. Bull. 30, 150.

Guillocheau, F., Simon, B., Baby, G., Bessin, P., Robin, C., Dauteuil, O., 2018. Planation surfaces as a record of mantle dynamics: the case example of Africa. Gondwana Res. 53, 82–98. https://doi.org/10.1016/j.gr.2017.05.015.

Gunnell, Y., Harbor, D.J., 2010. Butte detachment: how pre-rift geological structure and drainage integration drive escarpment evolution at rifted continental margins. Earth Surf. Process. Landforms 35, 1373–1385. https://doi.org/10.1002/esp.1973.

Hamza, V.M., Dias, F.J.S.S., Gomes, A.J.L., Terceros, Z.G.D., 2005. Numerical and functional representations of regional heat flow in South America. Phys. Earth Planet. In. 152, 223–256. https://doi.org/10.1016/j.pepi.2005.04.009.

Haq, B.U., 2014. Cretaceous eustasy revisited. Glob. Planet. Chang. 113, 44–58. https://doi.org/10.1016/j.gloplacha.2013.12.007.

Harman, R., Gallagher, K., Brown, R.W., Raza, A., Bizzi, L., 1998. Accelerated denudation and tectonic/geomorphic reactivation of the cratons of northeastern Brazil during the Late Cretaceous. J. Geophys. Res. 103, 27091–27105. https://doi.org/10.1029/98JB02524.

Heilbron, M., Duarte, B.P., Valeriano, C. de M., Simonetti, A., Machado, N., Nogueira, J.R., 2010. Evolution of reworked Paleoproterozoic basement rocks within the Ribeira belt (Neoproterozoic), SE-Brazil, based on U-Pb geochronology: implications for paleogeographic reconstructions of the São Francisco-Congo paleocontinent. Precambrian Res. 178, 136–148. https://doi.org/10.1016/j.precamres.2010.02.002.

Heilbron, M., Pedrosa-Soares, A.C., Neto, A.C.B., da Silva, L.C., Trouw, R., Janasi, V., 2004. Brasiliano orogens in southeast and south Brazil. In: Fuck, R.A., Trouw, R., Wienberg, R., Hackspacher, P.C. (Eds.), The 750-550 Ma Brasiliano Event of South America. Journal of the Virtual Explorer, Electronic Edition, vol. 17. Paper 4.

Hendriks, B.W.H., Redfield, T.F., 2006. Reply to: comment on "Apatite Fission Track and (U-Th)/He data from Fennoscandia: an example of underestimation of fission track annealing in apatite" by B. W. H. Hendriks and T. F. Redfield. Earth Planet. Sci. Lett. 248, 568–576. https://doi.org/10.1016/j.epsl.2006.06.022.

Hiruma, S.T., Riccomini, C., Modenesi-Gauttieri, M.C., Hackspacher, P.C., Hadler Neto, J.C., Franco-Magalhães, A.O.B., 2010. Denudation history of the Bocaina Plateau, Serra do Mar, southeastern Brazil: relationships to Gondwana breakup and passive margin development. Gondwana Res. 18, 674–687. https://doi.org/10.1016/j.gr.2010.03.001.

House, M.A., Farley, K.A., Stockli, D., 2000. Helium chronometry of apatite and titanite using Nd-YAG laser heating. Earth Planet. Sci. Lett. 183, 365–368. https://doi.org/10.1016/S0012-821X(00)00286-7.

Hu, J., Faccenda, M., Liu, L., 2017. Subduction-controlled mantle flow and seismic anisotropy in South America. Earth Planet. Sci. Lett. 470, 13–24. https://doi.org/10.1016/j.epsl.2017.04.027.

Hueck, M., Dunkl, I., Heller, B., Stipp Basei, M.A., Siegesmund, S., 2018. (U-Th)/He thermochronology and zircon radiation damage in the south American passive margin: thermal overprint of the Paraná LIP? Tectonics 1–18. https://doi.org/10.1029/2018TC005041.

Hurford, A.J., 1990. Standardization of fission track dating calibration: recommendation by the fission track working group of the I.U.G.S. Subcommission on geochronology. Chem. Geol. Isot. Geosci. Sect. 80, 171–178. https://doi.org/10.1016/0168-9622(90)90025-8.

Hurford, A.J., Green, P.F., 1982. A users' guide to fission track dating calibration. Earth Planet. Sci. Lett. 59, 343–354. https://doi.org/10.1016/0012- 821X(82)90136-4.

Hurford, A.J., Green, P.F., 1983. The Zeta age calibration of fission-track dating. Isot. Geosci. 1, 285–317. https://doi.org/10.1016/S0009-2541(83)80026-6.

Japsen, P., Bonow, J.M., Green, P.F., Cobbold, P.R., Chiossi, D., Lilletveit, R., Magnavita, L.P., Pedreira, A., 2012a. Episodic burial and exhumation in NE Brazil after opening of the South Atlantic. Bull. Geol. Soc. Am. 124, 800–816. https://doi.org/10.1130/B30515.1.

Japsen, P., Chalmers, J.A., Green, P.F., Bonow, J.M., 2012b. Elevated, passive continental margins: not rift shoulders, but expressions of episodic, post-rift burial and exhumation. Glob. Planet. Chang. 90–91, 73–86. https://doi.org/10.1016/j.gloplacha.2011.05.004.

Japsen, P., Green, P.F., Bonow, J.M., Erlström, M., 2016. Episodic burial and exhumation of the southern Baltic Shield: epeirogenic uplifts during and after breakup of Pangaea. Gondwana Res. 35, 357–377. https://doi.org/10.1016/j.gr.2015.06.005.

Jelinek, A.R., Chemale, F.J., van der Beek, P.A., Guadagnin, F., Cupertino, J.A., Viana, A., 2014. Denudation history and landscape evolution of the northern East-Brazilian continental margin from apatite fission-track thermochronology.

J. South Am. Earth Sci. 54, 158–181. https://doi.org/10.1016/j.jsames.2014.06.001.
Jonckheere, R.C., 2003a. On the densities of etchable fission tracks in a mineral and co-irradiated external detector with reference to fission-track dating of minerals. Chem. Geol. 200, 41–58. https://doi.org/10.1016/S0009-2541(03)00116-5.
Jonckheere, R.C., 2003b. On methodical problems in estimating geological temperature and time from measurements of fission tracks in apatite. Radiat. Meas. 36, 43–55. https://doi.org/10.1016/S1350-4487(03)00096-9.
Jonckheere, R.C., Enkelmann, E., Min, M., Trautmann, C., Ratschbacher, L., 2007. Confined fission tracks in ion-irradiated and step-etched prismatic sections of Durango apatite. Chem. Geol. 242, 202–217. https://doi.org/10.1016/j.chemgeo.2007.03.015.
Jonckheere, R.C., Van den haute, P., Ratschbacher, L., 2015. Standardless fission-track dating of the Durango apatite age standard. Chem. Geol. 417, 44–57. https://doi.org/10.1016/j.chemgeo.2015.09.014.
Jordan, Theresa, E., Isacks, B.L., Allmendinger, R.W., Brewer, J.A., Ramos, V.A., Ando, C.J., 1983. Andean tectonics related to geometry of subducted Nazca plate. Geol. Study Am. Bull. 94, 341–361. https://doi.org/10.1130/0016-7606(1984)95-877.
Karl, M., Glasmacher, U.A., Kollenz, S., Franco-Magalhães, A.O.B., Stockli, D.F., Hackspacher, P.C., 2013. Evolution of the South Atlantic passive continental margin in southern Brazil derived from zircon and apatite (U-Th-Sm)/He and fission-track data. Tectonophysics 604, 224–244. https://doi.org/10.1016/j.tecto.2013.06.017.
Ketcham, R.A., 2005. Forward and inverse modeling of low-temperature thermochronometry data. Rev. Mineral. Geochem. 58, 275–314. https://doi.org/10.2138/rmg.2005.58.11.
Ketcham, R.A., Carter, A., Donelick, R.A., Barbarand, J., Hurford, A.J., 2007a. Improved modeling of fission-track annealing in apatite. Am. Mineral. 92, 799–810. https://doi.org/10.2138/am.2007.2281.
Ketcham, R.A., Carter, A., Donelick, R.A., Barbarand, J., Hurford, A.J., 2007b. Improved measurement of fission-track annealing in apatite using c-axis projection. Am. Mineral. 92, 789–798. https://doi.org/10.2138/am.2007.2280.
Ketcham, R.A., Donelick, R.A., Carlson, W.D., 1999. Variability of apatite fission-track annealing kinetics. III. Extraploation to geological time scales. Am. Mineral. 84, 1235–1255. https://doi.org/10.2138/am.2006.464.
Kooi, H., Beaumont, C., 1994. Escarpment evolution on high-elevation rifted margins: insights derived from a surface process model that combines diffusion, advaction and reaction. J. Geophys. Res. 99, 12191–12209.
Leroy, M., Gueydan, F., Dauteuil, O., 2008. Uplift and strength evolution of passive margins inferred from 2-D conductive modelling. Geophys. J. Int. 172, 464–476. https://doi.org/10.1111/j.1365-246X.2007.03566.x.
Lima, C., Nascimento, E., Assumpção, M., 1997. Stress orientations in Brazilian sedimentary basins from breakout analysis: implications for force models in the South American plate. Geophys. J. Int. 130, 112–124.
Lima, C.C.U., Vilas Boas, G.S., Bezerra, F.H.R., 2006. Faciologia e análise tectônica preliminar da Formação Barreiras no litoral sul do Estado da Bahia, Brasil. Geol. Usp. Série Científica 6, 71–80 (in Portuguese).
Lourenço, F.S., Alkmim, F.F., Araújo, M.N.C. de, Romeiro, M.A.T., Matos, G.C. de, Crósta, A.P., 2016. The Piúma lineament, southern Espirito Santo: structural expression and tectonic significance. Brazilian J. Geol. 46, 531–546. https://doi.org/10.1590/2317-4889201620150038 (in Portuguese).
Maloney, K.T., Clarke, G.L., Klepeis, K.A., Quevedo, L., 2013. The Late Jurassic to present evolution of the Andean margin: drivers and the geological record. Tectonics 32, 1049–1065. https://doi.org/10.1002/tect.20067.
Marent, B.R., Valadão, R.C., Manfré, L.A., Albuquerque Nóbrega, R.A. de, 2018. Spatiality and evolution of the incision of river valleys from the relief dissection in the staggered steps of the southeast of Minas Gerais - Brazil. Rev. Bras. Geomorfol. 19, 709–719. https://doi.org/10.20502/rbg.v19i4.1366.
Martin, L., Suguio, K., 1992. Variation of coastal dynamics during the last 7000 years recorded in beach-ridge plains associated with river mouths: example from the central Brazilian coast. Palaeogeogr. Palaeoclimatol. Palaeoecol. 99, 119–140. https://doi.org/10.1016/0031-0182(92)90010-3.
McDannell, K.T., Zeitler, P.K., Janes, D.G., Idleman, B.D., Fayon, A.K., 2018. Screening apatites for (U-Th)/He thermochronometry via continuous ramped heating: He age components and implications for age dispersion. Geochem. Cosmochim. Acta 223, 90–106. https://doi.org/10.1016/j.gca.2017.11.031.
McIntyre, G.A., Brooks, C., Compston, W., Turek, A., 1966. The statistical assessment of Rb-Sr isochrons. J. Geophys. 71, 5459–5468. https://doi.org/10.1029/JZ071i022p05459.
McKenzie, D., 1978. Some remarks on the development of sedimentary basins. Earth Planet. Sci. Lett. 40, 25–32. https://doi.org/10.1016/0012-821X(78)90071-7.
Meesters, A.G.C.A., Dunai, T.J., 2002. Solving the production – diffusion equation for finite diffusion domains of various shapes Part II . Application to cases with a-ejection and nonhomogeneous distribution of the source. Chem. Geol. 186, 333–344. https://doi.org/10.1016/S0009-2541(01)00422-3.
Mello, C.L., Metelo, C.M.S., Suguio, K., Kohler, H.C., 1999. Quaternary sedimentation, neotectonics and the evolution of the Doce river middle valley lake system (Southeastern Brazil). Rev. do Inst. Geológico, IG São Paulo 20, 29–36. https://doi.org/10.5935/0100-929x.19990003 (in Portuguese).
Mendes, R.S., 2017. Petrografia, geoquímica, geologica isotópica e geocronologia dos diques máfios do sul do estado do Espírito Santo, orógeno Araçuaí. MSc Thesis. Universidade Federal de Minas Gerais, p. 82 (in Portuguese).
Milani, E.J., 2007. Cartas estratigráficas. Bol. Geociencias Petrobras 15 (2) (in Portuguese).
Miller, K., Mountain, G., Wright, J., Browning, J., 2011. A 180-million-year record of sea level and ice volume variations from continental margin and deep-sea isotopic records. Oceanography 24, 40–53. https://doi.org/10.5670/oceanog.2011.26.
Miller, K.G., Kominz, M.A., Browning, J.V., Wright, J.D., Mountain, G.S., Katz, M.E., Sugarman, P.J., Cramer, B.S., Christie-Blick, N., Pekar, S.F., 2005. The Phanerozoic record of global sea-level change. Science 84 310, 1293–1298. https://doi.org/10.1126/science.1116412.
Mohriak, W., Nemčok, M., Enciso, G., 2008. South Atlantic divergent margin evolution: rift-border uplift and salt tectonics in the basins of SE Brazil. Geol. Soc. London, Spec. Publ. 294, 365–398. https://doi.org/10.1144/SP294.19.
Mohriak, W.U., 2003. Bacias sedimentares da margem continental Brasileira. In: Bizzi, L.A., Schobbenhaus, C., Vidotti, C., Goncalves, J.H. (Eds.), Geologia, Tectonica e Recursos Minerais Do Brasil. CPRM, Brasilia, pp. 87–165 (in Portuguese).
Morais Neto, J.M., Hegarty, K.A., Karner, G.D., Alkmim, F.F., 2009. Timing and mechanisms for the generation and modification of the anomalous topography of the Borborema Province, northeastern Brazil. Mar. Pet. Geol. 26, 1070–1086. https://doi.org/10.1016/j.marpetgeo.2008.07.002.
Nachtergaele, S., De Pelsmaeker, E., Glorie, S., Zhimulev, F., Jolivet, M., Danišík, M., Buslov, M.M., De Grave, J., 2018. Meso-Cenozoic tectonic evolution of the Talas-Fergana region of the Kyrgyz Tien Shan revealed by low-temperature basement and detrital thermochronology. Geosci. Front. 9. https://doi.org/10.1016/j.gsf.2017.11.007.
Noce, C.M., Pedrosa-Soares, A.C., da Silva, L.C., Armstrong, R., Piuzana, D., 2007. Evolution of polycyclic basement complexes in the Araçuaí Orogen, based on U-Pb SHRIMP data: implications for Brazil-Africa links in Paleoproterozoic time. Precambrian Res. 159, 60–78. https://doi.org/10.1016/j.precamres.2007.06.001.
Novais, L.C.C., Teixera, L.B., Neves, M.T., Todarte, J.B.M., Almeida, J.C.H., Valeriano, C.M., 2014. Novas ocorrências de diques de diabásio na faixa Colatina-ES: estruturas rútpeis associadas e implicações tectônicas para as bacias de Campos e do Espírito Santo. Bol. Geociencias Petrobras 1, 191–194 (in Portuguese).
Novo, T.A., Pedrosa-Soares, A., Vieira, V.S., Dussin, I., da Silva, L.C., 2018. The Rio Doce Group revisited: an Ediacaran arc-related volcano-sedimentary basin, Araçuaí orogen (SE Brazil). J. South Am. Earth Sci. 85, 345–361. https://doi.org/10.1016/j.jsames.2018.05.013.
Ojeda, H.A.O., 1982. Structural framework, stratigraphy and evolution of Brazilain marginal basins. Am. Assoc. Petrol. Geol. Bull. 66, 732–749.
Oliveira, K.S.S., Quaresma, V. da S., 2017. Temporal variability in the suspended sediment load and streamflow of the Doce River. J. South Am. Earth Sci. 78, 101–115. https://doi.org/10.1016/j.jsames.2017.06.009.
Owen, S.C., 2014. Geological Origins of Sugarloaf Mountains in Eastern Brazil and Their Environmental Significance as Refugia for the Mata Atlantica Rainforest. PhD thesis. University of Leicester, p. 337.
Pedrosa-Soares, A.C., Alkmim, F.F., Tack, L., Noce, C.M., Babinski, M., da Silva, L.C., Martins-Neto, M.A., 2008. Similarities and differences between the Brazilian and African counterparts of the Neoproterozoic Aracuai-west Congo orogen. Geol. Soc. London, Spec. Publ. 294, 153–172. https://doi.org/10.1144/SP294.9.
Pedrosa-Soares, A.C., Noce, C.M., Alkmim, F.F., da Silva, L.C., Babinski, M., Cordani, U.G., Castañeda, C., 2007. Orógeno Araçuaí : síntese do conhecimento 30 anos após almeida 1977. Geonomos 15, 1–16 (in Portuguese).
Pedrosa-Soares, A.C., Noce, C.M., Wiedemann, C.M., Pinto, C.P., 2001. The Araçuaí-West-Congo Orogen in Brazil: an overview of a confined orogen formed during Gondwanaland assembly. Precambrian Res. 110, 307–323. https://doi.org/10.1016/S0301-9268(01)00174-7.
Pereira Cruz, S.C., Figueiredo Barbosa, J.S., Pinto, M.S., Peucat, J.J., Paquette, J.L., Santos de Souza, J., de Souza Martins, V., Júnior, F.C., Carneiro, M.A., 2016. The Siderian-Orosirian magmatism in the Gavião Paleoplate, Brazil: U–Pb geochronology, geochemistry and tectonic implications. J. South Am. Earth Sci. 69, 43–79. https://doi.org/10.1016/j.jsames.2016.02.007.
Pérez-Díaz, L., Eagles, G., 2014. Constraining South Atlantic growth with seafloor spreading data. Tectonics 33, 1848–1873. https://doi.org/10.1002/2014TC003644.
Pérez-Gussinyé, M., Lowry, A.R., Watts, A.B., 2007. Effective elastic thickness of South America and its implications for intracontinental deformation. Geochem. Geophys. Geosyst. 8, 1–22. https://doi.org/10.1029/2006GC001511.
Peulvast, J.P., Claudino Sales, V., Bétard, F., Gunnell, Y., 2008. Low post-Cenomanian denudation depths across the Brazilian Northeast: implications for long-term landscape evolution at a transform continental margin. Glob. Planet. Chang. 62, 39–60. https://doi.org/10.1016/j.gloplacha.2007.11.005.
Potter, P.E., 1997. The Mesozoic and Cenozoic paleodrainage of South America: a natural history. J. South Am. Earth Sci. 10, 331–344. https://doi.org/10.1016/S0895-9811(97)00031-X.
Qin, Y., Alves, T.M., Constantine, J., Gamboa, D., 2016. Quantitative seismic geomorphology of a submarine channel system in SE Brazil (Espírito Santo Basin): scale comparison with other submarine channel systems. Mar. Pet. Geol. 78, 455–473. https://doi.org/10.1016/j.marpetgeo.2016.09.024.
Raab, M.J., Brown, R.W., Gallagher, K., Carter, A., Weber, K., 2002. Late Cretaceous reactivation of major crustal shear zones in northern Namibia: constraints from apatite fission track analysis. Tectonophysics 349, 75–92. https://doi.org/10.1016/S0040-1951(02)00047-1.
Ramos, V.A., Cristallini, E.O., Pérez, D.J., 2002. The pampean flat-slab of the central Andes. J. South Am. Earth Sci. 15, 59–78. https://doi.org/10.1016/S0895-9811(02)00006-8.

Reiners, P.W., Shuster, D.L., 2009. Thermochronology and landscape evolution. Phys. Today 62, 31–36. https://doi.org/10.1063/1.3226750.
Reis, Á.F.C., Bezerra, F.H.R., Ferreira, J.M., Do Nascimento, A.F., Lima, C.C., 2013. Stress magnitude and orientation in the Potiguar Basin, Brazil: implications on faulting style and reactivation. J. Geophys. Res. Solid Earth 118, 5550–5563. https://doi.org/10.1002/2012JB009953.
Ribeiro, M.C.S., 2007. Termocronologia e história denudacional da Serra do Mar e implicações no controle deposicional da Bacia de Santos. Inst. Geosci. Earth Sci. Univ. São Paulo, São Paulo, Brazil, p. 211 (in Portuguese).
Riccomini, C., 1989. O Rift Continental Do Sudeste Do Brasil. University of São Paulo, Brazil (in Portuguese).
Rossetti, D.F., Domingues, J.M.L., 2012. Tabuleiros costeiros. In: Barbosa, J.S.F. (Ed.), Geologia Da Bahia, Pesquisa e Atualização. CBPM/UFBA, pp. 365–394 (in Portuguese).
Rouby, D., Braun, J., Robin, C., Dauteuil, O., Deschamps, F., 2013. Long-term stratigraphic evolution of Atlantic-type passive margins: a numerical approach of interactions between surface processes, flexural isostasy and 3D thermal subsidence. Tectonophysics 604, 83–103. https://doi.org/10.1016/j.tecto.2013.02.003.
Sacek, V., Braun, J., Van Der Beek, P., 2012. The influence of rifting on escarpment migration on high elevation passive continental margins. J. Geophys. Res. Solid Earth 117. https://doi.org/10.1029/2011JB008547.
Salomon, E., Koehn, D., Passchier, C., Hackspacher, P.C., Glasmacher, U.A., 2015. Contrasting stress fields on correlating margins of the South Atlantic. Gondwana Res. 28, 1152–1167. https://doi.org/10.1016/j.gr.2014.09.006.
Schmitt, R. da S., Fragoso, R. de A., Collins, A.S., 2018. Suturing Gondwana in the Cambrian: the orogenic events of the final amalgamation. In: Siegesmund, S., Basei, M., Oyhantçabal, P., Oriolo, S. (Eds.), Geology of Southwest Gondwana. Springer, Cham, pp. 411–432. https://doi.org/10.1007/978-3-319-68920-3_15.
Scotese, C.R., 2004. A continental drift flipbook. J. Geol. 112, 729–741. https://doi.org/10.1086/424867.
Shuster, D.L., Flowers, R.M., Farley, K.A., 2006. The influence of natural radiation damage on helium diffusion kinetics in apatite. Earth Planet. Sci. Lett. 249, 148–161. https://doi.org/10.1016/j.epsl.2006.07.028.
Silva, L.C. da, Pedrosa-Soares, A.C., Armstrong, R., Pinto, C.P., Magalhães, J.T.R., Pinheiro, M.A.P., Santos, G.G., 2016. Disclosing the Paleoarchean to Ediacaran history of the São Francisco craton basement: the Porteirinha domain (northern Araçuaí orogen, Brazil). J. South Am. Earth Sci. 68, 50–67. https://doi.org/10.1016/j.jsames.2015.12.002.
Sobel, E.R., Seward, D., 2010. Influence of etching conditions on apatite fission-track etch pit diameter. Chem. Geol. 271, 59–69. https://doi.org/10.1016/j.chemgeo.2009.12.012.
Teixeira, L.B., Rodarte, J.B.M., 2003. Datações de Diques de Diabásios na Faixa Colatina (Rio de Janeiro) (in Portuguese).
Teixeira, W., Oliveira, E.P., Marques, L.S., 2017. Nature and evolution of the archean crust of the São Francisco craton. In: Heilbron, M., Cordani, U.G., Alkmim, F.F. (Eds.), São Francisco Craton, Eastern Brazil. Regional Geology Reviews. Springer, Cham, pp. 29–56. https://doi.org/10.1007/978-3-319-01715-0_3.
Tello Saenz, C., Hackspacher, P., Hadler Neto, J., Iunes, P., Guedes, S., Ribeiro, L.F., Paulo, S., 2003. Recognition of Cretaceous, Paleocene, and Neogene tectonic reactivation through apatite fission-track analysis in Precambrian areas of southeast Brazil: association with the opening of the south Atlantic Ocean. J. South Am. Earth Sci. 15, 765–774. https://doi.org/10.1016/S0895-9811(02)00131-1.
Tello Saenz, C.A., Hadler Neto, J.C., Iunes, P.J., Guedes, S., Hackspacher, P.C., Ribeiro, L.F.B., Paulo, S.R., Osorio, A.M., 2005. Thermochronology of the South American platform in the state of São Paulo, Brazil, through apatite fission tracks. Radiat. Meas. 39, 635–640. https://doi.org/10.1016/j.radmeas.2004.08.005.
Thompson, R.N., Gibson, S.A., Mitghell, J.G., Dickin, A.P., Leonardos, O.H., Brod, J.A., Greenwood, J.G., 1998. Migrating Cretaceous-Eocene magmatism in the serra do mar alkaline province, SE Brazil: melts from the deflected trindade mantle plume? J. Petrol. 39, 1493–1526. https://doi.org/10.1093/petroj/39.8.1493.
Torsvik, T.H., Rousse, S., Smethurst, M.A., 2009. A new scheme for the opening of the South Atlantic Ocean and the dissection of an Aptian salt basin. Geophys. J. Int. 183, 29–34. https://doi.org/10.1111/j.1365-246X.2010.04728.x.
Turner, J.P., Green, P.F., Holford, S.P., Lawrence, S.R., 2008. Thermal history of the Rio muni (west Africa)-NE Brazil margins during continental breakup. Earth Planet. Sci. Lett. 270, 354–367. https://doi.org/10.1016/j.epsl.2008.04.002.
Van der Beek, P., Andriessen, P., Cloetingh, S., 1995. Morphotectonic evolution of rifted continental margins: inferences from a coupled tectonic-surface processes model and fission track thermochronology. Tectonics 14, 406–421.
Vermeesch, P., 2008. Three new ways to calculate average (U-Th)/He ages. Chem. Geol. 249, 339–347. https://doi.org/10.1016/j.chemgeo.2008.01.027.
Vermeesch, P., 2010. HelioPlot, and the treatment of overdispersed (U-Th-Sm)/He data. Chem. Geol. 271, 108–111. https://doi.org/10.1016/j.chemgeo.2010.01.002.
Vermeesch, P., 2018. IsoplotR: a free and open toolbox for geochronology. Geosci. Front. 1479–1493. https://doi.org/10.1016/j.gsf.2018.04.001.
Vermeesch, P., Seward, D., Latkoczy, C., Wipf, M., Günther, D., Baur, H., 2007. α-Emitting mineral inclusions in apatite, their effect on (U-Th)/He ages, and how to reduce it. Geochem. Cosmochim. Acta 71, 1737–1746. https://doi.org/10.1016/j.gca.2006.09.020.
Wagner, G.A., Van den haute, P., 1992. Fission Track Dating. Kluwer Academic Publishers, Dordrecht.
Weissel, J.K., Karner, G.D., 1989. Flexural uplift of rift flanks due to mechanical unloading of the lithosphere during extension. J. Geophys. Res. Solid Earth 94, 13919–13950. https://doi.org/10.1029/JB094iB10p13919.
Wildman, M., Brown, R.W., Beucher, R., Persano, C., Stuart, F., Gallagher, K., Schwanethal, J., Carter, A., 2016. The chronology and tectonic style of landscape evolution along the elevated Atlantic continental margin of South Africa resolved by joint apatite fission track and (U-Th-Sm)/He thermochronology. Tectonics 35, 511–545. https://doi.org/10.1002/2015TC004042.
Zachos, J., Pagani, M., Sloan, L., Thomas, E., Billups, K., 2001. Trends , global rhythms , aberrations to present in global climate 65 Ma to present. Science 292, 686–693, 80-. https://doi.org/10.4103/0019-5049.84846.
Zeitler, P.K., Enkelmann, E., Thomas, J.B., Watson, E.B., Ancuta, L.D., Idleman, B.D., 2017. Solubility and trapping of helium in apatite. Geochem. Cosmochim. Acta 209, 1–8. https://doi.org/10.1016/j.gca.2017.03.041.
Zeitler, P.K., Herczeg, A.L., McDougall, I., Honda, M., 1987. U-Th-He dating of apatite: a potential thermochronometer. Geochem. Cosmochim. Acta 51, 2865–2868. https://doi.org/10.1016/0016-7037(87)90164-5.